Article Type: Original Article

Spatiotemporal distribution of ROS production, delivery and utilization in Arabidopsis root hairs

Lenka Kuběnová[1‡], Jan Haberland[1‡], Petr Dvořák[1], Jozef Šamaj[1], Miroslav Ovečka[1*]

[1]Department of Biotechnology, Faculty of Science, Palacký University Olomouc, Olomouc, Czech Republic

[*]**Correspondence:**
Miroslav Ovečka
email: miroslav.ovecka@upol.cz

[‡]These authors contributed equally to this work.

Running title: ROS and root hair tip growth

One sentence summary: High-resolution live-cell imaging of ROS production and subcellular localization in bulges and growing root hairs of Arabidopsis using CM-H_2DCFDA, CellRox Deep Red and Amplex Red selective probes.

Total word count: 6351

Number of Figures: 11

Of which color: 10

Keywords: Amplex Red, *Arabidopsis thaliana*, carboxy-2',7'-dichlorodihydrofluorescein diacetate, CellRox Deep Red, live cell imaging, root hairs, ROS, spinning disk

Abstract

Fluorescent selective probes for reactive oxygen species (ROS) detection in living cells are versatile tools for documentation of ROS production in developmental or stress reactions in plants. We employed staining of *Arabidopsis thaliana* with CM-H_2DCFDA, CellRox Deep Red and Amplex Red for functional characterization of spatiotemporal mode of ROS

production, delivery and utilization during root hair formation. Using high-resolution live-cell imaging and semi-quantitative analysis we characterized an ability of employed selective probes to reveal subcellular localization of ROS production and accumulation from bulge formation to tip growth of root hairs. The data show a sensitivity of CM-H_2DCFDA to ROS in cytoplasm, CellRox Deep Red to ROS in mitochondria and root hair-specific sensitivity of Amplex Red to ROS in apoplast and mitochondria. This dynamic and high-resolution study of ROS production and utilization opens new opportunities for precise speciation of particular ROS involved in root hair formation process.

Introduction

Root hairs are tubular outgrowths of specialized root epidermal cells, trichoblasts. A specific feature of the formation of root hairs is a spatiotemporal change in the polarity, driving the cell expansion. From the trichoblast expanding by a diffuse cell growth, a fundamental change in expansion mode occurs, and the root hair itself is further elongated only by polarized tip growth (Dolan et al., 1994; Baluška et al., 2000). Root hairs increase the total surface of the root, which significantly improves the absorption of water and nutrients. They also support the anchoring of the plant in the soil and enable symbiotic interactions with the beneficial microflora in the rhizosphere (Gilroy and Jones, 2000). The establishment, maintenance and regulation of the tip growth is conditioned by the maintenance of the polar organization of the tip-growing cell. Membrane transport processes, temporal and spatial regulation of exocytosis and endocytosis, as well as selective recycling of vesicles play a central role in this maintenance. Polar tip growth, including the maintenance of root hair polarity itself, requires regulated directional transport, dynamic properties of the cytoskeleton, maintenance of physiological gradients in the tip and, last but not least, signaling cascades (Baluška et al., 2000; Šamaj et al., 2006). Pollen tubes and root hairs are model objects for the study of tip growth in plants.

The formation of a bulge on the outer cell wall of the trichoblast represents a transitional phase between the diffuse growth of the epidermal cell and the tip growth of the root hair. From a mechanical, as well as a functional point of view, it is a rebuilding of the cell wall, which occurs primarily by local loosening of bonds. There is a local decrease in the pH of the cell wall (Bibikova et al., 1998), a localized increase in the concentration of proton ions in the cytoplasm (Bibikova et al., 1997). This is associated with an increase in xyloglucan endotransglycosylase activity (Vissenberg et al., 2001) and specific expression of expansin 7

and 10 in trichoblasts (Cho and Cosgrove, 2002). The creation of a proton gradient is also closely connected with the production of reactive oxygen species (Foreman et al., 2003). The mechanism regulating tip growth of root hairs requires a tip-focused gradient of Ca^{2+} in the cytosol, which regulates the activity of vesicular trafficking, generation of reactive oxygen species (ROS), and organization of the cytoskeleton in growing tip. Ca^{2+}- permeable ion channels are localized at the apical plasma membrane (Miedema et al., 2008) and ROS are generated by NADPH oxidase AtrbohC/RHD2. The ROS production is regulated by ROP GTPases (Foreman et al., 2003) and the whole process is interconnected by a positive feedback mechanism, which determines root hair polarity and tip growth (Carol et al., 2005; Takeda et al., 2008). Tip-focused accumulation of ROS is tightly associated also with tip growth of pollen tubes. AtABCG28, an ABC transporter, is responsible for ROS accumulation at the tip of the growing *Arabidopsis thaliana* pollen tubes (Do et al., 2019). In tip-growing cells, NADPH oxidases, highly regulated transmembrane proteins that use cytosolic NADPH, produce superoxide ($O_2^{\bullet-}$) at the apoplastic side of the plasma membrane, which is then converted to hydrogen peroxide (H_2O_2) by the activity of the superoxide dismutase in the apoplast (Demidchik, 2018). Hydrogen peroxide can diffuse to the cytoplasm of the tip-growing cells via aquaporins, forming there a tip-focused gradient of ROS (Bienert and Chaumont, 2014).

For quantitation of H_2O_2 in living cells quite extensively is used the oxidation of 2'-7' dichlorofluorescin (H_2DCF) to 2'-7'dichlorofluorescein (DCF). Important parameter is good permeability of the diacetate form, H_2DCFDA and its acetomethyl ester H_2DCFDA-AM through plasma membrane of living cells. Probes are taken up by cells and nonspecific cellular esterases cleave off the lipophilic groups, resulting in a trapping the charged compound inside the cell. Oxidation of H_2DCF by ROS in cells converts the molecule to 2',7' dichlorodihydrofluorescein (DCF), which is highly fluorescent. Although DCF was believed to be specific for H_2O_2, some evidences indicate that other ROS such as nitrate and hypochlorous acid can oxidize H_2DCF (Hoffman et al., 2008). However, albeit this probe can react with other ROS, due to its high sensitivity, it has been widely used to monitor H_2O_2 production in plants (Swanson et al., 2011). The CellRox Deep Red is a fluorescent reagent that detects superoxide and hydroxyl radicals (Alves et al., 2015). It is a cell-permeant dye weakly fluorescent while in a reduced state, however, it exhibits strong and photostable fluorescence upon oxidation by ROS. Amplex Red is a most commonly used fluorogenic substrate, which serves as hydrogen donors in conjugation with horseradish peroxidase (HRP)

enzyme to produce intensely fluorescent product. Amplex Red serves in this case a potent and sensitive probe, as increasing amounts of H_2O_2 in cells leads to increasing amounts of specific fluorescent product. Amplex Red is oxidized by H_2O_2 in the presence of HRP and converts to resorufin (Reszka et al., 2005).

In tip-growing cells, fluorescence localization of ROS using CMH_2DCFDA or $DCFH_2$-DA was quite commonly employed. In pollen tubes, it was utilized for H_2O_2 detection (Potocký et al., 2007; Do et al., 2019). The same approach was used for localization of ROS production in Arabidopsis roots upon salt stress-induced signal transduction (Leshem et al., 2007) and in root hairs of Arabidopsis upon treatment with LY294002, a phosphatidylinositol 3-kinase (PI3K) - specific inhibitor (Lee et al., 2008). Alternatively, to test the possibility that the ROS produced by mitochondria might influence the tip growth of pollen tubes, a CellRox Deep Red probe, detecting superoxide and hydroxyl radicals was used (Do et al., 2019). In the absence of ROS it remains in its reduced state with no fluorescence, which is rapidly induced upon oxidation during cellular oxidative stress. CellRox Deep Red can be used to measure cellular ROS in the cytoplasm because it detects hydroxyl better than superoxide (Alves et al., 2015). In our knowledge, Amplex Red was not used for study of ROS production, distribution and utilization during root hair formation process.

Sensitive fluorescent probes were so far not utilized for subcellular discrimination between ROS sources in growing root hairs. Mapping of the origin, subcellular location of the production and dynamics of ROS utilization during bulge formation and tip growth of root hairs has not been documented and remains unknown. In this study, live-cell imaging using high-resolution spinning disk fluorescence microscopy supplemented with semi-quantitative analysis was used for functional characterization of spatiotemporal mode of ROS production, delivery and utilization in Arabidopsis root hairs from bulge formation to tip growth.

Results

ROS detection by fluorescent probes in Arabidopsis root apex

Staining of *Arabidopsis thaliana* root apex with CM-H_2DCFDA, CellRox Deep Red and Amplex Red, probes for selective ROS detection in living cells, provided slightly different staining pattern. In the elongation and differentiation zones, all epidermal cells were stained with CM-H_2DCFDA, while prominent labeling appeared in bulges, short root hairs and apices of long growing root hairs (Supplemental Figure S1A). Staining with CellRox Deep Red led

to detection of considerably lower signal in root epidermal cells, although the signal in bulges, short root hairs and apices of long growing root hairs was still very high (Supplemental Figure S1B). Unlike these two probes, staining with Amplex Red left root epidermal cells virtually negative. However, short root hairs and apices of long growing root hairs were specifically labeled (Supplemental Figure S1C). The first screening analysis thus revealed that the staining pattern of these three ROS-selective probes may differ in *A. thaliana* root cells, and that root hairs are worth to test these probes for detailed subcellular qualitative and quantitative ROS distribution pattern.

ROS detection in bulges and root hairs

In developing bulges, staining with CM-H_2DCFDA revealed presence of relatively low signal, distributed evenly in cytoplasm without any preference to particular subcellular compartments (Figure 1A-F). At given frequency of image acquisition every 30 sec, it was possible to capture bulge development and further root hair tip growth. Evaluation of images acquired at three different time points (0 min, 5 min and 10 min from the beginning of imaging) revealed no change in pattern of CM-H_2DCFDA signal distribution in developing bulge (Figure 1A-F; Supplemental Movie S1). Overview of the root hair formation zone revealed a prominent labeling pattern observed in apices of long growing root hairs (Supplemental Figure S1A). Therefore, after documentation of signal intensity and distribution in bulges, we analyzed „long“ growing root hairs first, that reached the length of 200 µm or were longer at the time of imaging. In these „long“ root hairs, staining with CM-H_2DCFDA led to accumulation of specific signal in cytoplasm, which was particularly prominent in root hair subapical zone (Figure 1G-L). Analysis at time points 0 min, 5 min and 10 min from the beginning of imaging showed that with root hair tip growth the zone with highest signal slightly enlarged after staining with CM-H_2DCFDA (Figure 1G-L; Supplemental Movie S2). Analysis of signal distribution after staining with CM-H_2DCFDA in „short“ root hairs, annotated according their length in the range of 10-200 µm at the time of imaging, revealed the same pattern (Supplemental Figure S2).

After staining with CellRox Deep Red, resulting signal was localized in distinct oval compartments in developing bulges. The size, number and cellular distribution of ROS-positive compartments was not changed during bulge development, and this staining pattern was stable over recorded time points (Figure 2A-F; Supplemental Movie S3). In „long“ growing root hairs stained with CellRox Deep Red these compartments were distributed in

156 cytoplasm within the subapical zone and around the vacuole, but were absent in clear zone
157 (Figure 2G-L). The most prominent accumulation of these compartments was visible in root
158 hair subapical zone (Figure 2G-L). From the analysis at 0 min, 5 min and 10 min time points
159 from the beginning of imaging was apparent that number of ROS-positive compartments after
160 staining with CellRox Deep Red in root hair subapical zone increases (Figure 2H,J,L;
161 Supplemental Movie S4). The same localization pattern after staining with CellRox Deep Red
162 was observed in „short“ root hairs, reaching the length of 10-200 µm at the time of imaging
163 (Supplemental Figure S3).

164 Specific staining pattern for root hairs after application of Amplex Red was apparent from
165 overview imaging of the root hair formation zone (Supplemental Figure S1C). In higher
166 resolution, developing bulges were outlined by strong Amplex Red-specific signal at the
167 surface, suggesting the localization in apoplast (Figure 3A-F; Supplemental Movie S5). In the
168 stage of „long“ growing root hairs, the Amplex Red-specific signal also outlined root hairs at
169 the surface (Figure 3G,I,K). Analysis of „short“ root hairs, reaching the length of 10-200 µm
170 at the time of imaging revealed the same localization pattern (Supplemental Figure S4). In
171 addition, this peripheral signal was weaker at the apex, where typically cell wall is thin, and
172 considerably stronger at the surface of subapical and shank regions where cell wall gets
173 thicker (Figure 3H,J,L; Supplemental Movie S6), suggesting an apoplast localization. We
174 decided to proof this localization pattern using transgenic line carrying GFP-RHD2, a GFP-
175 tagged AtRBOHC/RHD2, which is localized in specialized vesicular compartments and apical
176 plasma membrane in root hairs (Kuběnová et al., 2022). In root hairs, stained for ROS with
177 Amplex Red before, plasmolysis using 300 mM Mannitol induced the protoplast visualized
178 by GFP-RHD2 detachment from the apical cell wall (Figure 3M). Amplex Red-induced
179 surface signal observed before at the apical and subapical regions of control non-plasmolyzed
180 root hairs (Figure 3G-L) appeared at the remaining apoplast upon protoplast detachment after
181 plasmolysis (Figure 3N,O). Interestingly, in addition of apoplastic signal localization, we
182 observed also intracellular compartments positive to Amplex Red staining of ROS (Figure
183 3G,I,K). The internalization of Amplex Red and the presence of subcellular compartments
184 positive to Amplex Red-based ROS detection was proved also by a pseudo-color-coded
185 visualization of signal distribution (Figure 3H,J,L). The presence of intracellular
186 compartments positive to Amplex Red-based ROS detection was confirmed also by a
187 plasmolysis experiment (Figure 3N,O), indicating relatively high level of intracellular ROS
188 levels detectable by Amplex Red in growing root hairs after plasmolysis.

Semi-quantitative analysis of ROS distribution

We analyzed semi-quantitatively fluorescence signal distribution in apical parts of developing bulges and growing root hairs after ROS staining with CM-H_2DCFDA, CellRox Deep Red and Amplex Red probes. We characterized a mean fluorescence intensity distribution measured along a line oriented longitudinally at the apex of bulges and root hairs that was 10 µm long and reached up to the apical cell wall (Supplemental Movie S7). We analyzed data separately from bulges, as well as from „short“ and „long“ growing root hairs, and the mean fluorescence intensities were measured and analyzed at three time points (0 min, 5 min and 10 min) of imaging. Mean fluorescence intensity distribution of CM-H_2DCFDA revealed no differences among three recorded time points in bulges and growing root hairs (Figure 4A-C), however, the fluorescence intensity gradually increased (Figure 4A-C) with the lowest level in bulges and highest level in „long“ root hairs (Figure 4D; Supplemental Movie S8,S9). This analysis also revealed that CM-H_2DCFDA-specific signal was distributed equally in the subapical region, however decreasing considerably in apical clear zone and vanishing at apical plasma membrane and cell wall (Figure 4A-D; Supplemental Figure S5A). In bulges and root hairs stained with CellRox Deep Red the mean fluorescence intensity distribution showed rather an oscillating profile (Figure 4E-G), which followed ROS localization pattern in distinct subcellular compartments (Figure 2). Due to active movement of ROS-positive compartments, fluctuations in mean fluorescence intensities occurred and was obvious among recorded time points at 0 min, 5 min and 10 min (Figure 4E-G). In comparison to bulges, the mean fluorescence intensities considerably increased in growing root hairs (Figure 4H; Supplemental Movie S10,S11). Similarly to CM-H_2DCFDA-staining pattern, the signal intensity after CellRox Deep Red staining decreased in the apical clear zone and was considerably low at apical plasma membrane and cell wall (Figure 4E-H; Supplemental Figure S5B). Mean fluorescence intensity distribution within the apex of bulges and growing root hairs after staining with Amplex Red was analyzed in the distance of 10 µm longitudinally from the apical cell wall (Figure 5A) and transversally in 8 µm long profile located in a distance of 5 µm from the apical cell wall (Figure 5B). Both fluorescence intensity measurements revealed prominent signal located at the apical cell wall (longitudinally) and lateral cell wall at the subapical region. At the apex, it was apparent in bulges (Figure 5C), „short“ (Figure 5D) and „long“ (Figure 5E) growing root hairs, and there were no differences found among three time points (0 min, 5 min and 10 min) of imaging (Figure 5C-E). However, mean fluorescence intensity was lowest in bulges and higher in

„short“ and „long“ growing root hairs (Figure 5F; Supplemental Movie S12,S13). Lateral cell wall measured at the subapical region in a distance of 5 µm from the apex, provided the trend which was very similar, showing strong peak at the cell wall in „short“ (Figure 5G) and „long“ (Figure 5H) growing root hairs, while in „short“ growing root hairs the peak was more prominent (Figure 5I). Consistently with data presented in profiles (Figure 5), the average data of signal intensity after Amplex Red staining corroborated localized high cell wall staining pattern in bulges and growing root hairs (Supplemental Figure S5C).

ROS detection in root hair mutants

To reveal the relationship between subcellular sources of ROS generation and mechanism of root hair tip growth, we analyzed root hair mutants with phenotype of short root hairs (bulges) that are unable to elongate by tip growth. First one bears a loss-of-function mutations in the *AtRBOHC/RHD2* locus (*rhd2-1* mutant) resulting in missing tip-focused ROS and Ca^{2+} gradients (Schiefelbein and Somerville, 1990; Foreman et al., 2003). The second one, *der1-3* mutant, bears a single-point mutation in the *ACTIN2* gene and is typical by an impairment of root hair elongation after bulge establishment (Ringli et al., 2002). Distribution of ROS in bulges of *rhd2-1* mutant after staining with CM-H_2DCFDA revealed very low signal in the cytoplasm that remained unchanged in recorded time points at 0 min, 5 min and 10 min of imaging (Figure 6A-F; Supplemental Movie S14). Unlike this situation, in bulges of *der1-3* mutant the fluorescence signal after staining with CM-H_2DCFDA was considerably stronger (Figure 6G,I,K; Supplemental Movie S15) and exhibited visual increase in recorded time points at 0 min, 5 min and 10 min of imaging (Figure 6H,J,L). Comparison of differences in mean fluorescence intensities after CM-H_2DCFDA staining, measured along a 10 µm line oriented longitudinally at the central part of bulges among *rhd2-1* and *der1-3* mutants, and in respective Col-0 and C24 wild-types revealed normal level of ROS signal intensity in *der1-3* mutant, which was considerable reduced in *rhd2-1* mutant (Figure 6M). Differences in mean fluorescence intensities after CM-H_2DCFDA staining in Col-0 and C24 wild-types were negligible in „short“ root hairs and higher level of mean fluorescence intensity in C24 was found in „long“ root hairs (Supplemental Figure S6A,B). Staining of ROS with CellRox Deep Red in mutants showed similar pattern as observed in bulges of wild-type. CellRox Deep Red-dependent ROS localization in distinct compartments moving in the cytoplasm was observed in bulges of both *rhd2-1* (Figure 7A-F; Supplemental Movie S16) and *der1-3* (Figure 7G-L; Supplemental Movie S17) mutants. Analysis of mean fluorescence intensities after CellRox Deep Red staining, measured along a 10 µm line oriented longitudinally at the central part of

bulges, revealed a scattered pattern, among which data from *rhd2-1* and *der1-3* mutants fluctuated similarly as in respective Col-0 and C24 wild-types (Figure 6M). In „short“ root hairs CellRox Deep Red staining did not show any differences between Col-0 and C24 wild-types, while in „long“ root hairs higher level of mean fluorescence intensity was found in C24 (Supplemental Figure S6C,D). Staining root hair bulges with Amplex Red provided almost negative results in *rhd2-1* mutant (Figure 8A-F; Supplemental Movie S18), while in *der1-3* mutant showed signal strongly outlining the surface of bulges (Figure 8G-L; Supplemental Movie S19). Mean fluorescence intensities after Amplex Red staining, measured along a 10 µm line oriented longitudinally at the central part of bulges, revealed that signal intensity in peripheral cell wall was strong in *der1-3* mutant and its related C24 wild-type, while Col-0 wild type expressed lower cell wall staining (Figure 8M). Importantly, *rhd2-1* mutant contained only negligible amount of ROS detectable by Amplex Red in cell wall of bulges (Figure 8M). In growing root hairs, cell wall-localized ROS signal after Amplex Red staining was more or less uniform in Col-0 and C24 wild-types (Supplemental Figure S6E,F).

Subcellular identity of ROS-positive compartments in root hairs

Localization of ROS in subcellular compartments after CellRox Deep Red and Amplex Red staining prompted us to define their nature by a colocalization analysis with known subcellular molecular markers. We used transgenic lines carrying i) GFP-RHD2, a GFP-tagged AtRBOHC/RHD2 (Kuběnová et al., 2022), ii) GFP-RabA1d marker for early endosomal/TGN compartments (Ovečka et al., 2010; Berson et al., 2014; von Wangenheim et al., 2016), iii) RabF2a-YFP marker of late endosomes (von Wangenheim et al., 2016), and iv) GFP-tagged mitochondria-targeting sequence of the N terminus of the F1-ATPase g-subunit (Niwa et al., 1999). ROS-positive compartments after CellRox Deep Red staining were distributed in whole root hairs in exception of the clear zone (Figure 9A,D,G,J). GFP-RHD2 locates to vesicular compartments belonging to early endosomes/TGN and to apical plasma membrane in root hairs (Figure 9A). Detailed view did not revealed a colocalization between ROS-positive compartments and GFP-RHD2 (Figure 9B), which was confirmed by a fluorescence intensity profile measurement through the compartments (Figure 9C). GFP-RabA1d was located in early endosomal/TGN compartments accumulated in the apical and subapical regions of root hairs (Figure 9D) and detailed analysis showed no colocalization with ROS-positive compartments (Figure 9E,F). RabF2a-YFP decorated larger late endosomes located mainly away of the apical and subapical regions of root hairs (Figure 9G). Higher magnification (Figure 9H) and a semi-quantitative profile measurement of

288 fluorescence signal intensities (Figure 9I) revealed no colocalization with ROS-positive
289 compartments. On the other hand, mitochondria identified by a mitochondrial GFP marker
290 showed the same size, shape and distribution pattern as ROS-positive compartments after
291 CellRox Deep Red staining (Figure 9J). A high degree of their colocalization was revealed by
292 both high magnification visualization (Figure 9K) and fluorescence intensity profile
293 measurements (Figure 9L).

294 Staining of root hairs with Amplex Red resulted in strong signal accumulation in cell wall
295 (Figure 3,5), but there was also obvious internalization of the probe and localization of ROS
296 by Amplex Red intracellularly (Figure 3H,L,N,O). To characterize the nature of intracellular
297 ROS-positive compartments after Amplex Red staining, we used the same colocalization
298 analysis. GFP-RHD2 in moving vesicular compartments (Figure 10A) did not colocalize with
299 ROS-positive compartments (Figure 10B,C). Early endosomal/TGN compartments marked by
300 GFP-RabA1d (Figure 10D) did not show the colocalization with ROS-positive compartments
301 as well (Figure 10E,F). The same results we received after colocalization of late endosomes
302 marked by RabF2a-YFP (Figure 10G) with ROS-positive compartments, it was negative
303 (Figure 10H,I). Importantly, a mitochondrial GFP marker identifying mitochondria (Figure
304 10J) showed overlapping distribution pattern with ROS-positive compartments after Amplex
305 Red staining (Figure 10K), which was proved by fluorescence intensity profile measurements
306 (Figure 10L). Colocalization analysis thus revealed that distinct compartments in developing
307 bulges and growing root hairs, highly positive to ROS after CellRox Deep Red staining are
308 mitochondria, and unique intracellular ROS-positive compartments after Amplex Red
309 staining, which is specific probe for ROS detection in apolpast, are indeed mitochondria as
310 well.

311 **Discussion**

312 Production, accumulation and localization of ROS in plant cells can be documented by
313 different methods. Popular are small-molecule fluorescent probes that are able to assess ROS
314 produced within cells, or even those that are released from cells. Because ROS represent a
315 range of chemical oxygen species with different properties, investigating ROS in biological
316 systems should selectively concern a particular ROS of interest. It is obvious that most of the
317 ROS probes do not capture quantitatively intracellular ROS formed under investigation. In
318 addition, specific reaction of the probe with the ROS generated in cells may interfere with

319 redox state in cells and indeed, affect experimental results (Murphy et al., 2022). Small-
320 molecule fluorescent probes are thus frequently used for ROS documentation, however, some
321 of their limitations such as selectivity, ability to quantify, linearity in response or some
322 possible artefacts should be considered (Kalyanaraman et al., 2012). Fluorescent probe 2',7'-
323 dichlorodihydrofluorescein (DCFH), its diacetate form (CM-H_2DCFDA), rapidly enters living
324 cells, and is used as an indicator of ROS in living cells. After its passive diffusion into the
325 cytoplasm, its acetate groups are cleaved by esterases and chloromethyl groups react with
326 glutathione and other thiols. It is subsequently oxidized to highly fluorescent product 2',7'-
327 dichlorofluorescein (DCF), which is entrapped inside the cell. This allows long-term
328 observation (Eruslanov and Kusmartsev, 2010). It is often used as a probe for the indirect
329 detection of H_2O_2 and oxidative stress (Kalyanaraman et al., 2012; Winterbourn, 2014).
330 However, oxidation to the fluorescent 2',7'-dichlorofluorescein could be catalyzed by several
331 ROS, and thus this probe is not always considered as specific for any particular ROS (Murphy
332 et al., 2022). It is very important to assess physiologically relevant conditions for cells before
333 ROS are going to be detected, visualized and measured. In our system, undisturbed tip growth
334 of root hairs, reflected by speed of growth and root hair morphology, secured biologically
335 relevant conditions in our experiments. A slight increase in ROS levels during imaging of
336 growing root hairs could be induced by the energy of lasers used in long-term observation
337 (Khan et al., 2015). Light is absorbed by organic molecules such as flavins and they degrade
338 in reaction with oxygen (Gorgidze et al., 1998; Hockberger et al., 1999; Rösner et al., 2016).
339 This process then produces ROS, mainly superoxide and hydroxyl radicals (Icha et al., 2017),
340 which cause the formation of DCF (Eruslanov and Kusmartsev, 2010) and the subsequent
341 increase in fluorescence intensity. However, the increasing amount of ROS during root hair
342 elongation is indeed typical for the course of their tip growth. Generation of ROS is important
343 for the import of Ca^{2+} ions, which are required for apical cell expansion (Foreman et al., 2003;
344 Carrol et al., 2005).

345 Level of H_2O_2 in the apoplast can be determined by oxidizing substrates for peroxidases, such
346 as frequently used Amplex Red. In addition of H_2O_2 content created in the apoplast, this probe
347 can be sensitive to H_2O_2 released from cell, since H_2O_2 is able to cross plasma membranes,
348 directly or via aquaporins. Importantly, the measurement could be a real balance between
349 H_2O_2 being produced, or removed by intracellular enzymes, and it may reflect the rate of
350 diffusion not only inside, but also outside of the cell. Therefore, Amplex Red with horseradish

351 peroxidase can be used for detection of H_2O_2 release from cells if other reducing agents or
352 peroxidase substrates are absent (Murphy et al., 2022).

353 Process of ROS production in cells, in relation to their subcellular source, reflects either a
354 passive production, where ROS are generated as by-products of metabolic pathways during
355 photosynthesis and respiration, or active production by oxidases for signaling, such as
356 RBOHs, respiratory burst oxidase homologues. The cellular sources of ROS production for
357 signaling can thus be defined as extrinsic (in apoplast and/or cell wall), cytoplasmic and
358 nuclear, or organellar (in chloroplasts, mitochondria, or peroxisomes) (Yao et al., 2002; Datt
359 et al., 2003; Mittler et al., 2022). The NADPH oxidases are plasma membrane proteins and
360 for their activity they accept electrons from NADPH. This happens at the cytosolic side of the
361 plasma membrane with the formation of molecular oxygen at the outer side, leading to the
362 production of apoplastic superoxide (Mittler, 2017; Smirnoff and Arnaud, 2019). Fluorescent
363 probe 2',7'-dichlorodihydrofluorescein-diacetate (H_2DCFDA) that is particularly sensitive to
364 H_2O_2, was used for time course of production and intracellular localization of ROS in
365 Arabidopsis root tips exposed to salt stress. The fact that non-fluorescent H_2DCFDA became
366 entrapped by the surrounding membrane once hydrolyzed by the intracellular esterases to
367 H_2DCF, which after reaction with H_2O_2 produced fluorescent dichlorofluorescein (DCF), was
368 utilized for ROS localization in endosomes (Leshem et al., 2007). In Arabidopsis it was
369 established that phosphatidylinositol 3-phosphate (PtdIns(3)P) and phosphatidylinositol 3-
370 kinase (PI3K) as important factors for normal root hair growth. Essential processes such as
371 vesicle trafficking and ROS formation, were compromised in the presence of LY294002, a
372 PI3K-specific inhibitor. ROS generation inside of endosomes and endocytosis were
373 indispensable for tip growth. Preincubation of seedlings with LY294002 considerably reduced
374 ROS levels in the root hairs, as estimated using the dye 2',7'-dichlorodihydrofluorescein-
375 diacetate (Lee et al., 2008). The use of the CellRox Deep Red, on the other hand, revealed that
376 the signal was excluded from the apex of growing pollen tube. Instead, it was distributed
377 throughout the body of the pollen tube. This analysis suggested that the tip-localized ROS
378 signal does not represent superoxide or hydroxyl radicals, but H_2O_2 in growing pollen tubes.
379 Such results indicate that ROS generated from mitochondria are not major contributors to
380 specific spatial distribution of H_2O_2 in the apex of growing pollen tubes (Do et al., 2019).

381 Root hair tip growth is regulated to secure correct shape and size of bulges and elongating
382 root hairs. Factors such as Ca^{2+}, pH and ROS play an important role in this process (Mangano
383 et al., 2016). In growing root hairs, ROS are produced by RHD2 (ROOT HAIR DEFECTIVE

2), which is a plasma membrane-resident NADPH oxidase. ROS regulate polar root hair expansion through activation of calcium channels allowing Ca^{2+} uptake. Mutants *rhd2-1* are defective in Ca^{2+} uptake, have impaired cell expansion, causing a phenotype of very short root hairs (Foreman et al., 2003). Our results show that the *rhd2-1* mutant line possess a considerably lower amount of ROS in the bulge as analyzed by a CM-H_2DCFDA fluorescence. These results are not surprising, as a mutation of the *RHD2* gene targets the NADPH oxidase AtRBOHC/RHD2, responsible for the production of ROS in root hairs (Foreman et al., 2003). It proofs previous results that intracellular ROS levels in short root hairs of the *rhd2* mutant, detected using 2',7'-dichlorodihydrofluorescein-diacetate, were below the detection limit at pH 5 (Lee et al., 2008). Activity of AtRBOHC/RHD2 leads to generation of apoplastic $O_2^{\bullet-}$, from which H_2O_2 is subsequently produced by a reaction catalyzed by superoxide dismutase (SOD; Mangano et al., 2016). Our data show a dramatic reduction in the formation of apoplastic ROS, particularly H_2O_2, that has been clearly documented by Amplex Red staining. In turn, a reduction in the formation of apoplastic ROS can also result in reduced levels of H_2O_2 in the cytoplasm, reflected by lowering in fluorescence intensity after CM-H_2DCFDA staining. The actin cytoskeleton participates in the polar elongation of cells, and is indispensable also for determining the tip growth in root hairs (Zheng et al., 2009; Wang et al., 2010; Pei et al., 2012). Together with actin, indispensable is the activity of actin-binding proteins. Actin-depolymerization factor (ADF) and profilin are accumulated in the bulge and in the growing tips of root hairs, where they are responsible for the dynamic remodeling of the filamentous actin network (Staiger et al., 1997, Braun et al., 1999). A high degree of actin dynamics in the bulge selectively concentrates endomembranes and leads to the direction of vesicular transport preferentially to this subcellular domain (Baluška et al., 2000). Mutagenesis of the *ACTIN2* gene led to the isolation of *der1-3* (*deformed root hairs*) mutant line, which shows a phenotype of very short root hairs not able to elongate after a bulge formation (Ringli et al., 2002; Vaškebová et al., 2018). Determination of ROS related to bulge stage during the root hair formation process revealed, however, that ROS levels selectively detected by CM-H_2DCFDA and Amplex Red staining were not altered in *der1-3* mutant. It clearly shows that inability of root hairs to elongate in *rhd2-1* and *der1-3* mutants have principally different relationship to spatiotemporal distribution, production, delivery and utilization of ROS.

In conclusion, our high-resolution live-cell imaging provide a dynamic mapping of ROS in cytoplasm, mitochondria and apoplast, highlighting subcellular location of the production and

dynamics in tip-growth root hairs (Figure 11). This study also establish currently used fluorescent ROS probes, CM-H_2DCFDA, CellRox Deep Red and Amplex Red, for functional characterization of spatiotemporal mode of ROS production, delivery and utilization in Arabidopsis bulges and root hairs.

Materials and methods

Plant material and cultivation in vitro

Experiments were performed with plants of *Arabidopsis thaliana* wild types of the Col-0 and C24 ecotypes, *rhd2-1* mutant (Foreman *et al*., 2003) and *der1-3* mutant (Ringli *et al*., 2002) and stably transformed Arabidopsis lines carrying construct GFP-RHD2 for NADPH oxidase type C (Takeda *et al*., 2008), GFP-RabA1d for early endosomes/TGN (Ovečka *et al*., 2010; Berson et al., 2014; von Wangenheim et al., 2016), RabF2a-YFP fore late endosomes (von Wangenheim et al., 2016), and the GFP-tagged mitochondria-targeting sequence of the N terminus of the F1-ATPase g-subunit (Niwa et al., 1999). After surface-sterilization, the seeds of control, mutant and transgenic lines were planted on half-strength Murasige and Skoog (MS) medium (Murashige and Skoog, 1962) without vitamins, solidified with 0.6% (w/v) gellan gum (Alfa Aesar, Thermo Fisher Scientific, Heysham, UK). To synchronize seed germination, Petri dishes were stratified for 3 days at 4°C and then cultivated vertically in an environmental chamber at 21°C, 70% humidity, and 16-h/8-h light/dark cycle. The illumination intensity was 130 μmol $m^{-2}s^{-1}$.

Application of fluorescent probes for ROS detection

CM-H_2DCFDA, CellROX™ Deep Red and Amplex™ Red reagents (Thermo Fisher Scientific, Waltham, MA, USA) were used as vital probes for ROS detection in growing root hairs. At least in five independent plants per treatment, CM-H_2DCFDA (5 μmol.L^{-1}), CellROX ™ Deep Red (10 μmol.L^{-1}), and Amplex™ Red (1 μmol.L^{-1}) in modified liquid MS medium (Ovečka et al. 2014) were individually applied by perfusion directly to plantlets in the microscopic chamber. In total, 60 μL of the modified liquid MS medium with CM-H_2DCFDA, CellROX™ Deep Red, or Amplex™ Red was applied in 6 separate steps of 10 μL each. Plants were then observed using a spinning disk microscope. The root hairs were scanned at different times after perfusion of the probes. Several hairs were usually scanned consecutively, with at least 10 min pauses between scans to avoid induction of fluorescence caused by overloaded laser exposure.

Plasmolysis of root hairs

Transgenic plants carrying GFP-RHD2, 2- to 3-day-old were transferred to microscopic chambers containing liquid modified MS medium according to Ovečka *et al*. (2005, 2014). After manipulation with plants during sample preparation, the subsequent stabilization period for 24 h allowed undisturbed growth of the root and the formation of new root hairs. The plasmolysis was induced with 300 $mmol.L^{-1}$ solution of mannitol (Sigma-Aldrich, St Louis, MO, USA) by perfusion methods. Amplex™ Red Reagent (1 $\mu mol.L^{-1}$) was added to the mannitol solution. Total volume of solution was 100 µl divided into 10 steps of 10 µl applications. Plasmolysed root hairs were immediately observed by Airyscan microscope.

Epifluorescence microscopy

Plantlets of Col-0 plants (prepared in the microscopic chambers) were observed using an epifluorescence microscope Axio Imager M2 equipped with DIC optics and epifluorescence metal halide source illuminator HXP 120 V (Zeiss, Oberkochen, Germany), and analyzed using Zeiss ZEN 2012 Blue software (Zeiss, Germany). Root tips were labelled with fluorescent probes for ROS detection (CM-H_2DCFDA, CellROX ™ Deep Red and Amplex™ Red). Imaging was performed with N-Achroplan 5x/0.15 NA dry objective and documented with a Zeiss AxioCam ICm1 camera. A filter set providing a wavelength of 450-490 nm for the excitation and 515-565 nm for the emission at 200 ms exposure time was used to visualize the CM-H_2DCFDA signal. For the CellROX ™ Deep Red and Amplex™ Red, the filter set provided an excitation wavelength of 533-558 nm and an emission wavelength of 570-640 nm. The exposure time was set up to 1 s for both probes. The image scaling for all signals was 0.93 × 0.93 µm in x × y dimensions, and 15.12 µm in the z dimension. Final images were processed by orthogonal projection with weighted average function.

Spinning disk (SD) microscopy

Samples were prepared according to Ovečka *et al*. (2005, 2014), by transferring 2- to 3-d-old plants to microscopic chambers containing liquid modified MS medium. As the root hairs are very sensitive to stress during the manipulation, overnight cultivation for plant stabilization and undisturbed growth of the root and the formation of new root hairs was necessary. For quantitative and colocalization analyses a Cell Observer SD Axio Observer Z1 spinning disk microscope (Carl Zeiss,Germany) was used, equipped with alpha Plan-Apochromat 100×/1.57 NA DIC Korr oil immersion objective (Carl Zeiss, Germany). The samples were

imaged using an excitation laser line of 488 nm and emission filter BP525/50 for CM-H_2DCFDA and GFP signal detection, excitation laser line of 514 nm, and emission filter BP535/30 for YFP signal detection, excitation laser line of 639 nm and emission filter BP690/50 for CellROX™ Deep Red signal detection, and excitation laser line of 561 nm and emission filter BP629/62 for the Amplex™ Red signal detection. The excitation laser power level for all lasers used was set up to 50%, and the image scaling for all channels was 0.133 × 0.133 µm in x × y dimensions, and with the z dimension 0.63 µm for the GFP and CM-H_2DCFDA signal, 0.66 µm for the YFP channel, 0.75 µm for the CellROX™ Deep Red and Amplex™ Red signal. Images were acquired sequentially or simultaneously with two Evolve 512 EMCCD cameras (Photometrics) with an exposure time of 700 ms. The samples were scanned with 700 ms of exposure time for GFP, YFP and CM-H_2DCFDA signal, with 50 ms of exposure time for CellROX™ Deep Red signal, and with 500 ms of exposure time for Amplex™ Red signal (for quantitative analysis) or using a camera-streaming mode (for colocalization studies).

Airyscan confocal laser scanning microscopy (Airyscan CLSM)

Root hairs for ROS staining after plasmolysis were observed using a confocal laser scanning microscope LSM880 equipped with Airyscan (Carl Zeiss, Germany). Image acquisition was performed with a 20×/0.8 NA dry Plan-Apochromat objective (Carl Zeiss, Germany). The samples were imaged with an excitation laser line of 488 nm and BP420-480 + BP495-550 emission filters for GFP detection and an excitation laser line of 561 nm and BP420-480 + BP600-650 emission filters for Amplex™ Red detection. The laser power did not exceed 2% for GFP and 1% for Amplex™ Red of the available laser intensity range. The samples were scanned with 700 ms of exposure time for both signals using a 32 GaAsP detector. Pixel dwell time was set up to 1.6 µs, and with default settings of the gain level the image scaling was set up to 0.07 × 0.07 µm (x × y).

Data analysis and measurements

The signal intensity was analyzed using a spinning disk microscope. The root hairs were scanned for 10 min at 30 s intervals and sorted into groups according to developmental stages. For Col-0 and C24 lines at the stages of bulge, short root hair (10-200 µm) and long root hair (200+ µm), in *der1-3* and *rhd2-1* mutant lines at the bulge stage. Zen 3.3 blue edition software (Carl Zeiss, Germany) was used to obtain profiles for quantitative signal intensity

510 distribution of different fluorescent probes in growing root hairs. Intensities were measured in
511 single optical plane, in a 10 µm segment leading from the centre of the root hair to its tip
512 (Schematics, Supplemental Movie S7), always at the start of the scanning (0 min), in the
513 middle of the scanning (5 min) and at the end of the scanning (10 min).

514 Acquired data were processed in Microsoft Excel. Individually, the mean background
515 intensities were subtracted from the intensities in the segment. Root hairs with abnormal
516 intensities (exceeding double intensity over the average) were discarded from the statistics.
517 All charts were done in Microsoft Excel software and statistical analyses were obtained using
518 STATISTICA 13.4 (StatSoft) software using analysis of variance (ANOVA) and subsequent
519 Fisher's LSD tests ($P < 0.05$). The colocalization studies of fluorescence signals were
520 analyzed using a spinning disk microscope by simultaneous signal acquisition with two
521 independent Evolve 512 EMCCD cameras. The colocalization was analyzed in transgenic
522 lines GFP-RHD2, mito-GFP, GFP-RabA1d, and RabF2a-YFP in combination with the
523 fluorescent probes for ROS detection described above. Profiles for colocalization were
524 generated using Zen Blue 2014 software (Carl Zeiss, Germany) and graphically edited in
525 Microsoft Excel.

526 **Supplemental Data**

527 **Supplemental Figure S1.** Overview of ROS staining pattern in root hair formation zone
528 using different fluorescent probes.

529 **Supplemental Figure S2.** Distribution of ROS in root hairs after staining with CM-
530 H_2DCFDA.

531 **Supplemental Figure S3.** Distribution of ROS in root hairs after staining with CellRox Deep
532 Red.

533 **Supplemental Figure S4.** Distribution of ROS in root hairs after staining with Amplex Red.

534 **Supplemental Figure S5.** Average of fluorescence intensities in apical parts of bulges and
535 root hairs after ROS staining with CM-H_2DCFDA, CellRox Deep Red and Amplex Red.

536 **Supplemental Figure S6.** Fluorescence intensity profiles in apical parts of root hairs after
537 ROS staining with CM-H_2DCFDA, CellRox Deep Red and Amplex Red in wild-type Col-0
538 and C24 lines.

539 **Supplemental Movie S1.** Developing bulge of Col-0 wild-type imaged with CM-H_2DCFDA.

540 **Supplemental Movie S2.** Growing root hair of Col-0 wild-type imaged with CM-H_2DCFDA.

541 **Supplemental Movie S3.** Developing bulge of Col-0 wild-type imaged with CellRox Deep
542 Red.

543 **Supplemental Movie S4.** Growing root hair of Col-0 wild-type imaged with CellRox Deep
544 Red.

545 **Supplemental Movie S5.** Developing bulge of Col-0 wild-type imaged with Amplex Red.

546 **Supplemental Movie S6.** Growing root hair of Col-0 wild-type imaged with Amplex Red.

547 **Supplemental Movie S7.** Principle of semi-quantitative fluorescence signal intensity
548 measurement in profiles of 10 µm long from the center of the root hair to its tip.

549 **Supplemental Movie S8.** Semi-quantitative fluorescence signal intensity measurement in
550 bulge of Col-0 wild-type imaged with CM-H_2DCFDA.

551 **Supplemental Movie S9.** Semi-quantitative fluorescence signal intensity measurement in
552 root hair of Col-0 wild-type imaged with CM-H_2DCFDA.

553 **Supplemental Movie S10.** Semi-quantitative fluorescence signal intensity measurement in
554 bulge of Col-0 wild-type imaged with CellRox Deep Red.

555 **Supplemental Movie S11.** Semi-quantitative fluorescence signal intensity measurement in
556 root hair of Col-0 wild-type imaged with CellRox Deep Red.

557 **Supplemental Movie S12.** Semi-quantitative fluorescence signal intensity measurement in
558 bulge of Col-0 wild-type imaged with Amplex Red.

Supplemental Movie S13. Semi-quantitative fluorescence signal intensity measurement in root hair of Col-0 wild-type imaged with Amplex Red.

Supplemental Movie S14. Semi-quantitative fluorescence signal intensity measurement in bulge of *rhd2-1* mutant imaged with CM-H_2DCFDA.

Supplemental Movie S15. Semi-quantitative fluorescence signal intensity measurement in bulge of *der1-3* mutant imaged with CM-H_2DCFDA.

Supplemental Movie S16. Semi-quantitative fluorescence signal intensity measurement in bulge of *rhd2-1* mutant imaged with CellRox Deep Red.

Supplemental Movie S17. Semi-quantitative fluorescence signal intensity measurement in bulge of *der1-3* mutant imaged with CellRox Deep Red.

Supplemental Movie S18. Semi-quantitative fluorescence signal intensity measurement in bulge of *rhd2-1* mutant imaged with Amplex Red.

Supplemental Movie S19. Semi-quantitative fluorescence signal intensity measurement in bulge of *der1-3* mutant imaged with Amplex Red.

Funding

This work was supported by the Czech Science Foundation GAČR (project Nr. 19-18675S) and by student project IGA_PrF_2022_014 from PU Olomouc.

Authors' contributions

LK and JH performed experiments, microscopic data acquisition and analysis, semi-quantitative evaluation and statistical analyses. PD analyzed data from fluorescent probe labeling. JŠ and MO contributed to the experimental plan and data interpretation. MO wrote the manuscript with input from all co-authors. JŠ provided infrastructure and secured funding.

Conflicts of interest

The authors declare that they have no conflict of interest.

583 **Data Availability**

584 Data that support the findings of this study are available from the corresponding author upon
585 reasonable request.

586 **Figure legends**

587 **Figure 1. Distribution of ROS in bulges and root hairs after staining with CM-**
588 **H_2DCFDA. A-F.** Developing bulge imaged at time points of 0 min **(A,D)**, 5 min **(B,E)** and 10
589 min **(C,F)** of growth. **G-L.** Growing root hairs imaged at time points of 0 min **(G,H)**, 5 min
590 **(I,J)** and 10 min **(K,L)**. Semi-quantitative fluorescence intensity distribution **(D-F,H-L)** is
591 visualized in a pseudo-color-coded scale, where dark blue represents minimal intensity and
592 pale red represents maximum intensity **(**insets in **D** and **H)**. Growing root hairs were
593 annotated as „long", reaching the length of 200 µm and more at the time of imaging. Image
594 acquisition at the time point 0 min started 110 min and 154 min after probe application in
595 bulge **(A-F)** and „long" root hair (G-L), respectively. Scale bar = 10 µm **(A-L)**.

596 **Figure 2. Distribution of ROS in bulges and root hairs after staining with CellRox Deep**
597 **Red. A-F.** Developing bulge imaged at time points of 0 min **(A,D)**, 5 min **(B,E)** and 10 min
598 **(C,F)** of growth. **G-L.** Growing root hairs imaged at time points of 0 min **(G,H)**, 5 min **(I,J)**
599 and 10 min **(K,L)**. Semi-quantitative fluorescence intensity distribution **(D-F,H-L)** is
600 visualized in a pseudo-color-coded scale, where dark blue represents minimal intensity and
601 pale red represents maximum intensity **(**insets in **D** and **H)**. Growing root hairs were
602 annotated as „long", reaching the length of 200 µm and more at the time of imaging. Image
603 acquisition at the time point 0 min started 37 min and 47 min after probe application in bulge
604 **(A-F)** and „long" root hair **(G-L)**, respectively. Scale bar = 10 µm **(A-L)**.

605 **Figure 3. Distribution of ROS in bulges and root hairs after staining with Amplex Red.**
606 **A-F.** Developing bulge imaged at time points of 0 min **(A,D)**, 5 min **(B,E)** and 10 min **(C,F)**
607 of growth. **G-L.** Growing root hairs imaged at time points of 0 min **(G,H)**, 5 min **(I,J)** and 10
608 min **(K,L)**. Semi-quantitative fluorescence intensity distribution **(D-F,H-L)** is visualized in a
609 pseudo-color-coded scale, where dark blue represents minimal intensity and pale red
610 represents maximum intensity **(**insets in **D** and **H)**. Growing root hairs were annotated as
611 „long", reaching the length of 200 µm and more at the time of imaging. Image acquisition at
612 the time point 0 min started 28 min and 47 min after probe application in bulge **(A-F)** and
613 „long" root hair **(G-L)**, respectively. **M-O.** Root hair of transgenic line carrying GFP-RHD2
614 plasmolyzed by 300 mM mannitol **(M)** that was before stained with Amplex Red **(N)**, shown
615 in merged image **(O)**. Scale bar = 10 µm **(A-O)**.

616 **Figure 4. Fluorescence intensity profiles in apical parts of bulges and root hairs after**
617 **ROS staining with CM-H_2DCFDA and CellRox Deep Red. A-D.** Mean fluorescence
618 intensity distribution of CM-H_2DCFDA measured along a 10 µm line oriented longitudinally
619 at the central part, reaching the apical cell wall (schematically illustrated in Materials and
620 Methods) in bulges **(A)** „short" **(B)** and „long" **(C)** growing root hairs. Mean fluorescence
621 intensities were measured at 0 min, 5 min and 10 min of imaging **(A-C)**. **D.** Differences in

mean fluorescence intensities of CM-H_2DCFDA measured during root hair development from bulges to „long“ root hairs. **E-H.** Mean fluorescence intensity distribution of CellRox Deep Red measured along a 10 µm line oriented longitudinally at the central part, reaching the apical cell wall in bulges **(E)**, „short“ **(F)** and „long“ **(G)** growing root hairs. Mean fluorescence intensities were measured at 0 min, 5 min and 10 min of imaging **(E-G)**. **H.** Differences in mean fluorescence intensities of CellRox Deep Red measured during root hair development from bulges to „long“ root hairs.

Figure 5. Fluorescence intensity profiles in apical parts of bulges and root hairs after ROS staining with Amplex Red. A-B. Location of a profile 10 µm long for fluorescence intensity measurement in the longitudinal direction **(A)** and a profile 8 µm long in a distance of 5 µm from the apical cell wall for fluorescence intensity measurement in the transversal direction **(B)**. **C-F.** Mean fluorescence intensity distribution of Amplex Red measured along a 10 µm line oriented longitudinally at the central part, reaching the apical cell wall **(**according to **A)** in bulges **(C)**, „short“ **(D)** and „long“ **(E)** growing root hairs. **F.** Differences in mean fluorescence intensities of Amplex Red measured in longitudinal direction during root hair development from bulges to „long“ root hairs. **G-I.** Mean fluorescence intensity distribution of Amplex Red measured transversally **(**according to **B)** in „short“ **(G)** and „long“ **(H)** growing root hairs. **I.** Differences in mean fluorescence intensities of Amplex Red measured in transversal direction between „short“ and „long“ root hairs. Mean fluorescence intensities were measured at 0 min, 5 min and 10 min of imaging. Scale bar = 10 µm **(A,B)**.

Figure 6. Distribution of ROS after staining with CM-H_2DCFDA in bulges of *rhd2-1* and *der1-3* mutants. A-F. Bulge in *rhd2-1* mutant illustrated at time points of 0 min **(A,B)**, 5 min **(C,D)** and 10 min **(E,F)** of imaging. **G-L.** Bulge in *der1-3* mutant illustrated at time points of 0 min **(G,H)**, 5 min **(I,J)** and 10 min **(K,L)** of imaging. Semi-quantitative fluorescence intensity distribution in *rhd2-1* mutant **(B,D,F)** and *der1-3* mutant **(H,J,L)** is visualized in a pseudo-color-coded scale, where dark blue represents minimal intensity and pale red represents maximum intensity **(**insets in **B** and **H)**. Image acquisition at the time point 0 min started 101 min and 49 min after probe application in *rhd2-1* mutant and *der1-3* mutant, respectively. M. Differences in mean fluorescence intensities of CM-H_2DCFDA in *rhd2-1* and *der1-3* mutants, and respective Col-0 and C24 wild-types, measured along a 10 µm line oriented longitudinally at the central part of bulges. Scale bar = 10 µm **(A-L)**.

Figure 7. Distribution of ROS after staining with CellRox Deep Red in bulges of *rhd2-1* and *der1-3* mutants. A-F. Bulge in *rhd2-1* mutant illustrated at time points of 0 min **(A,B)**, 5 min **(C,D)** and 10 min **(E,F)** of imaging. **G-L.** Bulge in *der1-3* mutant illustrated at time points of 0 min **(G,H)**, 5 min **(I,J)** and 10 min **(K,L)** of imaging. Semi-quantitative fluorescence intensity distribution in *rhd2-1* mutant **(B,D,F)** and *der1-3* mutant **(H,J,L)** is visualized in a pseudo-color-coded scale, where dark blue represents minimal intensity and pale red represents maximum intensity **(**insets in **B** and **H)**. Image acquisition at the time point 0 min started 74 min and 7 min after probe application in *rhd2-1* mutant and *der1-3* mutant, respectively. **M.** Differences in mean fluorescence intensities of CellRox Deep Red in *rhd2-1* and *der1-3* mutants, and respective Col-0 and C24 wild-types, measured along a 10 µm line oriented longitudinally at the central part of bulges. Scale bar = 10 µm **(A-L)**.

Figure 8. Distribution of ROS after staining with Amplex Red in bulges of *rhd2-1* and *der1-3* mutants. A-F. Bulge in *rhd2-1* mutant illustrated at time points of 0 min **(A,B)**, 5 min **(C,D)** and 10 min **(E,F)** of imaging. **G-L.** Bulge in *der1-3* mutant illustrated at time points of 0 min **(G,H)**, 5 min **(I,J)** and 10 min **(K,L)** of imaging. Semi-quantitative fluorescence intensity distribution in *rhd2-1* mutant **(B,D,F)** and *der1-3* mutant **(H,J,L)** is visualized in a pseudo-color-coded scale, where dark blue represents minimal intensity and pale red represents maximum intensity **(**insets in **B** and **H)**. Image acquisition at the time point 0 min started 5 min and 29 min after probe application in *rhd2-1* mutant and *der1-3* mutant, respectively. **M.** Differences in mean fluorescence intensities of Amplex Red in *rhd2-1* and *der1-3* mutants, and respective Col-0 and C24 wild-types, measured along a 10 µm line oriented longitudinally at the central part of bulges. Scale bar = 10 µm **(A-L)**.

Figure 9. Colocalization analysis of subcellular molecular markers in root hairs with compartments accumulating ROS after staining with CellRox Deep Red. A-C. Colocalization with transgenic line for visualization of vesicular compartments containing GFP-RHD2, a GFP-tagged AtRBOHC/RHD2. **D-F.** Colocalization with transgenic line carrying early endosomal marker GFP-RabA1d. **G-I.** Colocalization with transgenic line carrying late endosomal marker RabF2a-YFP. **J-L.** Colocalization with transgenic line carrying GFP-tagged mitochondria. Overview of root hairs carrying molecular markers (in green) and ROS-accumulating compartments (in magenta) after CellRox Deep Red staining **(A,D,G,J)**. Detailed images of compartments containing carrying molecular markers and ROS **(B,E,H,K)** from the white boxes shown in **(A,D,G,J)**. Fluorescence intensity profiles **(C,F,I,L)** of fluorescence signals of molecular markers (green lines) and ROS-containing compartments (magenta lines) along the interrupted white lines shown in **(B,E,H,K)**. Arrows in **(B,C,E,F,H,I,K,L)** indicate the position of the compartments. Scale bar = 5 µm **(A,D,G,J)**, 1 µm **(B,E,H,K)**.

Figure 10. Colocalization analysis of subcellular molecular markers in root hairs with compartments accumulating ROS after staining with Amplex Red. A-C. Colocalization with transgenic line for visualization of vesicular compartments containing GFP-RHD2, a GFP-tagged AtRBOHC/RHD2. **D-F.** Colocalization with transgenic line carrying early endosomal marker GFP-RabA1d. **G-I.** Colocalization with transgenic line carrying late endosomal marker RabF2a-YFP. **J-L.** Colocalization with transgenic line carrying GFP-tagged mitochondria. Overview of root hairs carrying molecular markers (in green) and ROS-accumulating compartments (in magenta) after Amplex Red staining **(A,D,G,J)**. Detailed images of compartments containing carrying molecular markers and ROS **(B,E,H,K)** from the white boxes shown in **(A,D,G,J)**. Fluorescence intensity profiles **(C,F,I,L)** of fluorescence signals of molecular markers (green lines) and ROS-containing compartments (magenta lines) along the interrupted white lines shown in **(B,E,H,K)**. Arrows in **(B,C,E,F,H,I,K,L)** indicate the position of the compartments. Scale bar = 5 µm **(A,D,G,J)**, 0.5 µm **(B,E,H,K)**.

Figure 11. Model of subcellular ROS localization in root hairs with CM-H_2DCFDA, CellRox Deep Red and Amplex Red. CM-H_2DCFDA represents a sensitive probe for ROS (mainly H_2O_2) in the cytoplasm. CellRox Deep Red localizes specifically ROS in mitochondria. Amplex Red serves as a highly sensitive marker for root hair-specific

706 apoplastic ROS (mainly H_2O_2). In addition, root hairs are able to internalize Amplex Red,
707 which sensitively detects H_2O_2 in mitochondria.

708

709 **References**

710 **Alves MBR, de Andrade AFC, de Arruda RP, Batissaco L, Florez- Rodriguez SA, et al.**
711 (2015) An Efficient Technique to Detect Sperm Reactive Oxygen Species: The CellRox Deep
712 Red® Fluorescent Probe. Biochem Physiol **4**:157

713 **Baluška F, Salaj J, Mathur J, Braun M, Jasper F, Šamaj J, Chua NH, Barlow PW,**
714 **Volkmann D** (2000) Root hair formation: F-actin-independent tip growth is initiated by local
715 assembly of proflin-supported F-actin meshworks accumulated within expansin-enriched
716 bulges. Dev Biol **227**: 618-632

717 **Berson T, Wangenheim D, Takáč T, Šamajová O, Rosero A, Ovečka M, Komis G,**
718 **Stelzer EH, Šamaj J** (2014) Trans-Golgi network localized small GTPase RabA1d is
719 involved in cell plate formation and oscillatory root hair growth. BMC Plant Biol **14**: 252

720 **Bibikova TN, Zhigilei A, Gilroy S** (1997) Root hair growth in Arabidopsis thaliana is
721 directed by calcium and an endogenous polarity. Planta **203**: 495–505

722 **Bibikova TN, Jacob T, Dahse I, Gilroy S** (1998) Localized changes in apoplastic and
723 cytoplasmic pH are associated with root hair development in *Arabidopsis thaliana*.
724 Development **125**: 2925–2934

725 **Bienert GP, Chaumont F** (2014) Aquaporin-facilitated transmembrane diffusion of
726 hydrogen peroxide. Biochim Biophys Acta **1840**: 1596–1604

727 **Braun M, Baluška F, von Witsch M, Menzel D** (1999) Redistribution of actin, profilin and
728 phosphatidylinositol-4,5-bisphosphate (PIP2) in growing and maturing root hairs. Planta **209**:
729 435–443

730 **Carol RJ, Takeda S, Linstead P, Durrant MC, Kakesova H, Derbyshire P, Drea S,**
731 **Žárský V, Dolan L** (2005) A RhoGDP dissociation inhibitor spatially regulates growth in
732 root hair cells. Nature **438**: 1013-1016

733 **Datt JF, Pellinen R, Beeckman T, Van De Cotte B, Langebartels C, Kangasjervi J, Inze**
734 **D, Van Breusegem F** (2003) Changes in hydrogen peroxide homeostasis trigger an active
735 cell death process in tobacco. Plant J **33**: 621–629

736 **Demidchik V** (2018) ROS-activated ion channels in plants: Biophysical characteristics,
737 physiological functions and molecular nature. Int J Mol Sci **19**: E1263

738 **Do THT, Choi H, Palmgren M, Martinoia E, Hwang JU, Lee Y** (2019) Arabidopsis
739 ABCG28 is required for the apical accumulation of reactive oxygen species in growing pollen
740 tubes. Proc Nat Acad Sci USA **116**: 12540–12549

741 **Dolan L, Duckett C, Grierson C, Linstead P, Schneider K, Lawson E, Dean C, Poethig S,**
742 **Roberts K** (1994) Clonal relationships and cell patterning in the root epidermis of
743 Arabidopsis. Development **120**: 2465-2474

744 **Eruslanov E, Kusmartsev S** (2010) Identification of ROS using oxidized DCFDA and flow-
745 cytometry. Methods in Molecular Biology **594**: 57-72

746 **Foreman J, Demidchik V, Bothwell JH, Mylona P, Miedema H, Torres MA, Linstead P,**
747 **Costa S, Brownlee C, Jones JD, Davies JM, Dolan L** (2003) Reactive oxygen species
748 produced by NADPH oxidase regulate plant cell growth. Nature **422**: 442–446

749 **Gilroy S, Jones DL** (2000) Through form to function: root hair development and nutrient
750 uptake. Trends Plant Sci **5**: 56–60

751 **Gorgidze LA, Oshemkova SA, Vorobjev IA** (1998) Blue light inhibits mitosis in tissue
752 culture cells. Bioscience Reports **18**: 215-224

753 **Hockberger PE, Skimina TA, Centonze VE, Lavin C, Chu S, Dadras S, Reddy JK,**
754 **White JG** (1999) Activation of flavin-containing oxidases underlies light-induced production
755 of H_2O_2 in mammalian cells. Proc Nat Acad Sci USA **96**: 6255-6260.

756 **Hoffman A, Spetner LM, Burke M** (2008) Ramifications of a Redox Switch within a
757 Normal Cell; Its Absence in a Cancer Cell. Free Radical Biology and Medicine **45**: 265–268

758 **Cho H-T, Cosgrove DJ** (2002) Regulation of root hair initiation and expansin gene
759 expression in Arabidopsis. Plant Cell **14**: 3237–3253

760 **Icha J, Weber M, Waters JC, Norden C** (2017) Phototoxicity in live fluorescence
761 microscopy, and how to avoid it. BioEssays **39(8)**

762 **Kalyanaraman B, Darley-Usmar V, Davies KJ, Dennery PA, Forman HJ, Grisham MB,**
763 **Mann GE, Moore K, Roberts LJ 2nd, Ischiropoulos H** (2012) Measuring reactive oxygen
764 and nitrogen species with fluorescent probes: challenges and limitations. Free Radical
765 Biology & Medicine **52**: 1-6

766 **Khan I, Tang E, Arany P** (2015) Molecular pathway of near-infrared laser phototoxicity
767 involves ATF-4 orchestrated ER stress. Scientific Reports **5**:10581

768 **Kuběnová L, Tichá M, Šamaj J, Ovečka M** (2022) ROOT HAIR DEFECTIVE 2 vesicular
769 delivery to the apical plasma membrane domain during Arabidopsis root hair
770 development. Plant Physiol **188**: 1563-1585

771 **Lee Y, Bak G, Choi Y, Chuang WI, Cho HT, Lee Y** (2008) Roles of Phosphatidylinositol
772 3-Kinase in Root Hair Growth. Plant Physiol **147**: 624–635

773 **Leshem Y, Seri L, Levine A** (2007) Induction of phosphatidylinositol 3-kinase-mediated
774 endocytosis by salt stress leads to intracellular production of reactive oxygen species and salt
775 tolerance. Plant J **51**: 185–197

776 **Mangano S, Juárez SPD, Estevez JM** (2016) ROS Regulation of Polar Growth in Plant
777 Cells. Plant Physiol **171**: 1593-1605

Miedema H, Demidchik V, Véry AA, Bothwell JH, Brownlee C, Davies JM (2008). Two voltage-dependent calcium channels co-exist in the apical plasma membrane of *Arabidopsis thaliana* root hairs. New Phytologist **179**: 378-385

Mittler R (2017) ROS are good. Trends Plant Sci **22**: 11–19

Mittler R, Zandalinas SI, Fichman Y, Van Breusegem F (2022) Reactive oxygen species signalling in plant stress responses. Nature Rev Mol Cell Biol **23**: 663-679

Murphy MP, Bayir H, Belousov V, Chang CJ, Davies KJA, Davies MJ, Dick TP, Finke T, Forman HJ, Janssen-Heininger Y, et al., (2022) Guidelines for measuring reactive oxygen species and oxidative damage in cells and *in vivo*. Nat Metabolism **4**: 651–662

Niwa Y, Hirano T, Yoshimoto K, Shimizu M, Kobayashi H (1999) Non-invasive quantitative detection and applications of nontoxic, S65T-type green fluorescent protein in living cells. Plant J **18**: 455–463

Ovečka M, Berson T, Beck M, Derksen J, Šamaj J, Baluška F, Lichtscheidl IK (2010) Structural sterols are involved in both the initiation and tip growth of root hairs in *Arabidopsis thaliana*. Plant Cell **22**: 2999–3019

Ovečka M, Lichtscheidl I, Šamaj J (2014) Live microscopy analysis of endosomes and vesicles in tip-growing root hairs. Methods Mol Biol **1209**: 31–44

Pei W, Du F, Zhang Y, He T, Ren H (2012) Control of the actin cytoskeleton in root hair development. Plant Sci **187**: 10–18

Potocký M, Jones MA, Bezvoda R, Smirnoff N, Žárský V (2007) Reactive oxygen species produced by NADPH oxidase are involved in pollen tube growth. New Phytol **174**: 742–751

Reszka KJ, Wagner BA, Burns CP, Britigan BE (2005) Effects of peroxidase substrates on the Amplex red/peroxidase assay: antioxidant properties of anthracyclines. Anal Biochem **342**: 327-337

Ringli C, Baumberger N, Diet A, Frey B, Keller B (2002) ACTIN2 is essential for bulge site selection and tip growth during root hair development of Arabidopsis. Plant Physiol **129**: 1464-1472

Rösner J, Liotta A, Angamo EA, Spies C, Heinemann U, Kovács R (2016) Minimizing photodecomposition of flavin adenine dinucleotide fluorescence by the use of pulsed LEDs. Journal of Microscopy **264**: 215-223

Schiefelbein JW, Somerville C (1990) Genetic control of root hair development in Arabidopsis thaliana. Plant Cell **2**: 235–243

Smirnoff N, Arnaud D (2019) Hydrogen peroxide metabolism and functions in plants. New Phytol **221**: 1197–1214

Staiger CJ, Gibbon BC, Kovar DR, Zonia LE (1997) Profilin and actin depolymerizing factor: modulators of actin organization in plants. Trends Plant Sci **2**: 275–281

Swanson SJ, Choi WG, Chanoca A, Gilroy S (2011) In vivo imaging of Ca2+, pH, and reactive oxygen species using fluorescent probes in plants. Annu Rev Plant Biol **62**: 273–297

Šamaj J, Müller J, Beck M, Böhm N, Menzel D (2006) Vesicular trafficking, cytoskeleton and signalling in root hairs and pollen tubes. Trends Plant Sci **11**: 594-600

Takeda S, Gapper C, Kaya H, Bell E, Kuchitsu K, Dolan L (2008). Local positive feedback regulation determines cell shape in root hair cells. Science **319**: 1241–1244

Vaškebová L, Šamaj J, Ovečka M (2018) Single-point ACT2 gene mutation in the Arabidopsis root hair mutant der1-3 affects overall actin organization, root growth and plant development. Ann Bot **122**: 889-901

Vissenberg K, Fry SC, Verbelen JP (2001) Root hair initiation is coupled to a highly localized increase of xyloglucan endotransglycosylase action in Arabidopsis roots. Plant Physiol **127**: 1125–1135

von Wangenheim D, Rosero A, Komis G, Šamajová O, Ovečka M, Voigt B, Šamaj J (2016) Endosomal interactions during root hair growth. Front Plant Sci **6**: 1262

Wang Y, Zhu Y, Ling Y, Zhang H, Liu P, Baluška F, Šamaj J, Lin J, Wang Q (2010) Disruption of actin filaments induces mitochondrial Ca^{2+} release to the cytoplasm and $[Ca^{2+}]c$ changes in Arabidopsis root hairs. BMC Plant Biol **10**: 53

Winterbourn CC (2014) The challenges of using fluorescent probes to detect and quantify specific reactive oxygen species in living cells. Biochimica et Biophysica Acta **1840**: 730-738

Yao N, Tada Y, Sakamoto M, Nakayashiki H, Park P, Tosa Y, Mayama S (2002) Mitochondrial oxidative burst involved in apoptotic response in oats. Plant J **30**: 567–579

Zheng M, Beck M, Müller J, Wang X, Wang Q, Baluška F, Logan DC, Šamaj J, Lin J (2009) Cytoskeleton-dependent mitochondrial movements in Arabidopsis root hairs. PLoS One **4:e5961**, 1–14

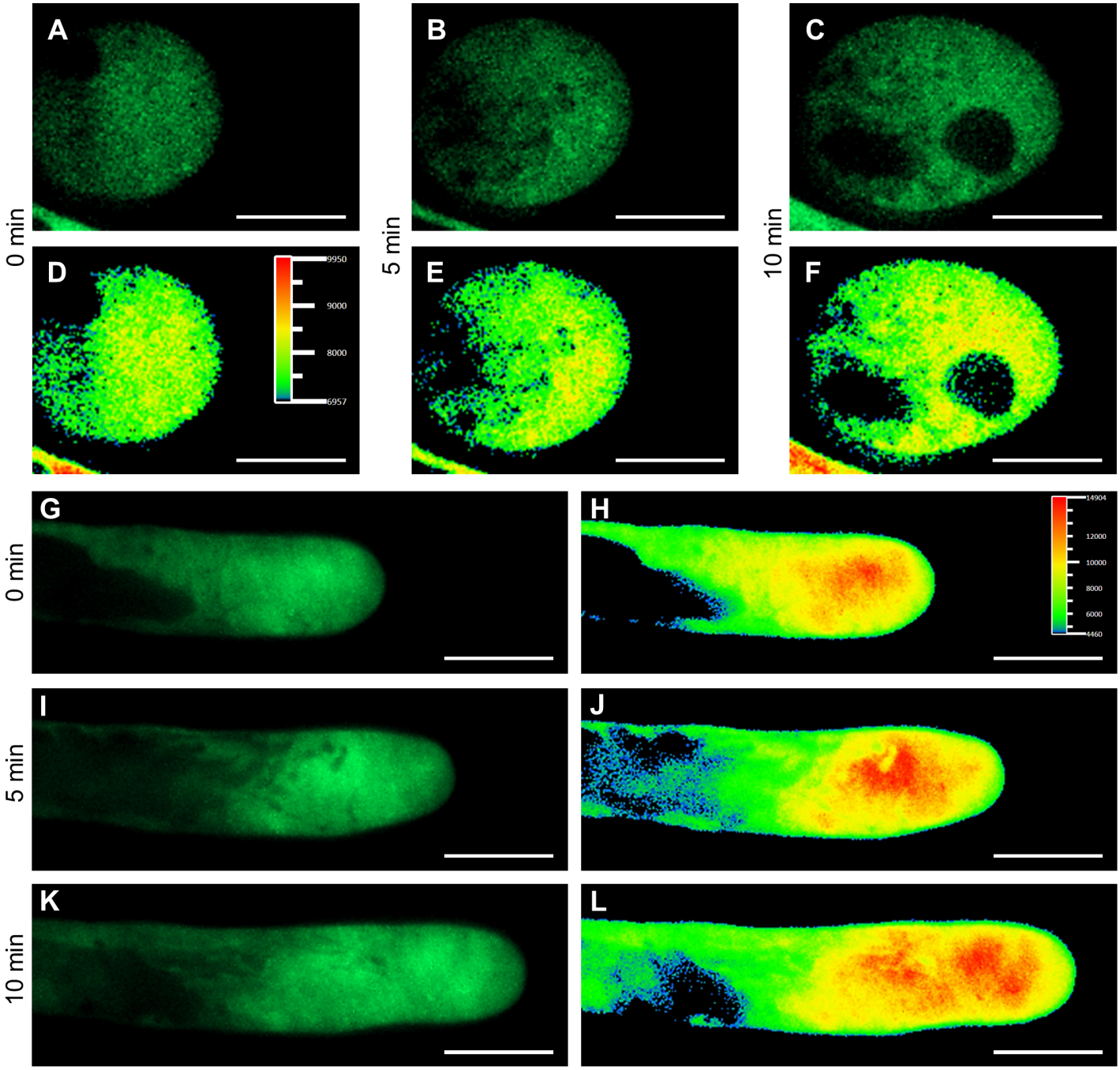

Figure 1. Distribution of ROS in bulges and root hairs after staining with CM-H_2DCFDA. A-F. Developing bulge imaged at time points of 0 min **(A,D)**, 5 min **(B,E)** and 10 min **(C,F)** of growth. **G-L.** Growing root hairs imaged at time points of 0 min **(G,H)**, 5 min **(I,J)** and 10 min **(K,L)**. Semi-quantitative fluorescence intensity distribution **(D-F,H-L)** is visualized in a pseudo-color-coded scale, where dark blue represents minimal intensity and pale red represents maximum intensity (insets in **D** and **H**). Growing root hairs were annotated as „long“, reaching the length of 200 µm and more at the time of imaging. Image acquisition at the time point 0 min started 110 min and 154 min after probe application in bulge **(A-F)** and „long“ root hair **(G-L)**, respectively. Scale bar = 10 µm **(A-L)**.

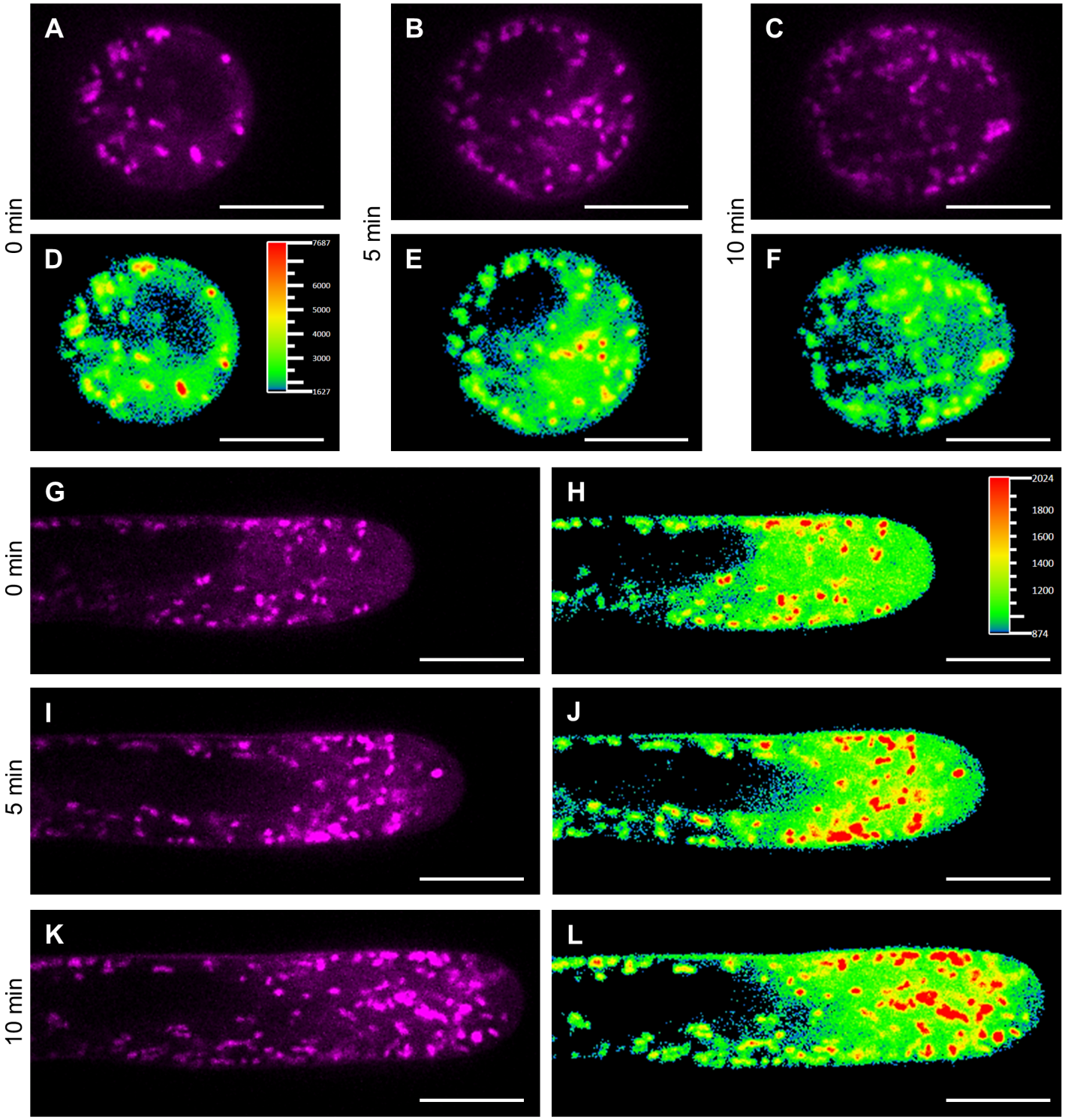

Figure 2. Distribution of ROS in bulges and root hairs after staining with CellRox Deep Red. A-F. Developing bulge imaged at time points of 0 min **(A,D)**, 5 min **(B,E)** and 10 min **(C,F)** of growth. **G-L.** Growing root hairs imaged at time points of 0 min **(G,H)**, 5 min **(I,J)** and 10 min **(K,L)**. Semi-quantitative fluorescence intensity distribution **(D-F,H-L)** is visualized in a pseudo-color-coded scale, where dark blue represents minimal intensity and pale red represents maximum intensity (insets in **D** and **H**). Growing root hairs were annotated as „long“, reaching the length of 200 µm and more at the time of imaging. Image acquisition at the time point 0 min started 37 min and 47 min after probe application in bulge **(A-F)** and „long“ root hair **(G-L)**, respectively. Scale bar = 10 µm **(A-L)**.

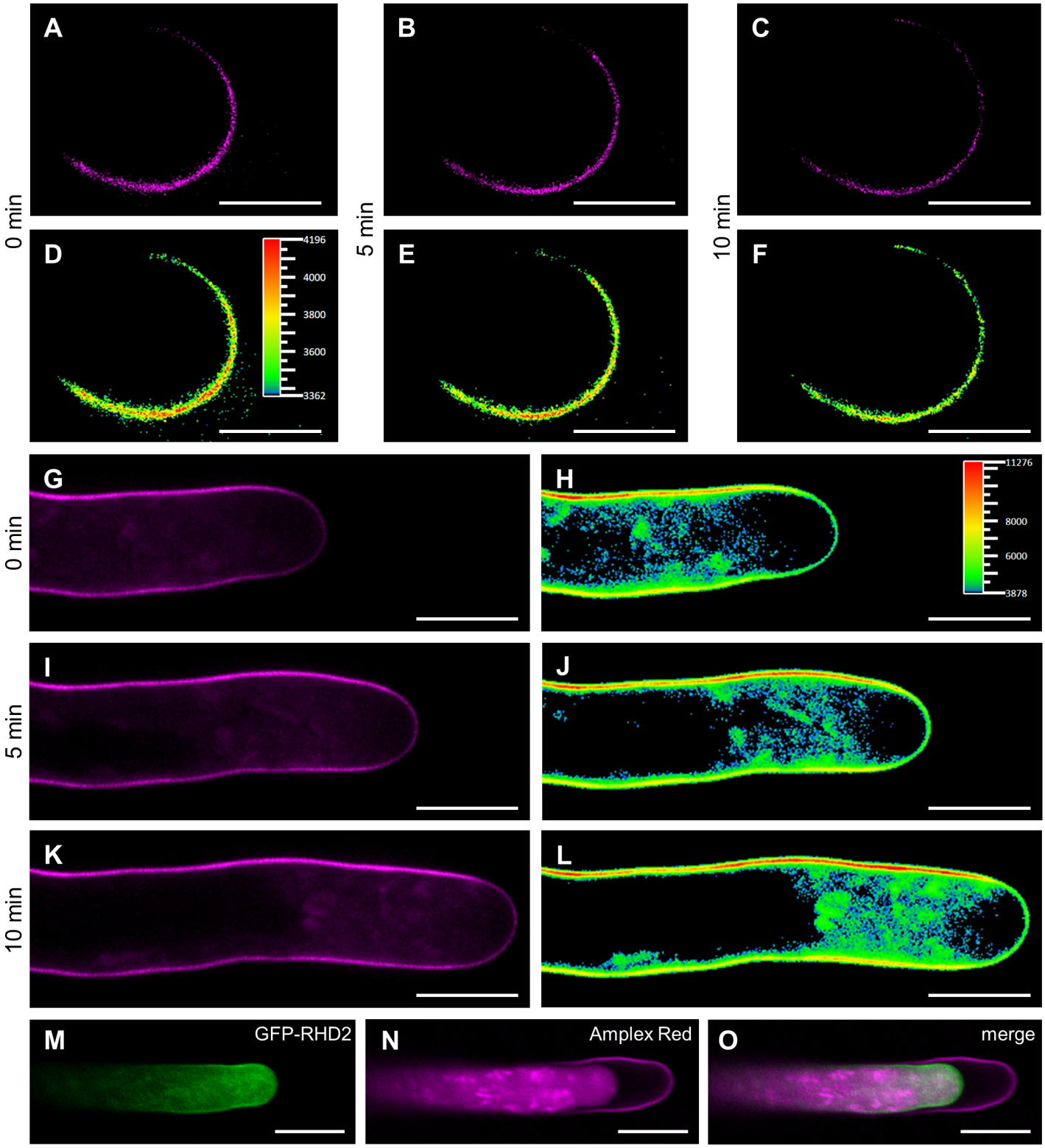

Figure 3. Distribution of ROS in bulges and root hairs after staining with Amplex Red. A-F. Developing bulge imaged at time points of 0 min **(A,D)**, 5 min **(B,E)** and 10 min **(C,F)** of growth. **G-L.** Growing root hairs imaged at time points of 0 min **(G,H)**, 5 min **(I,J)** and 10 min **(K,L)**. Semi-quantitative fluorescence intensity distribution **(D-F,H-L)** is visualized in a pseudo-color-coded scale, where dark blue represents minimal intensity and pale red represents maximum intensity (insets in **D** and **H**). Growing root hairs were annotated as „long“, reaching the length of 200 µm and more at the time of imaging. Image acquisition at the time point 0 min started 28 min and 47 min after probe application in bulge **(A-F)** and „long“ root hair **(G-L)**, respectively. **M-O.** Root hair of transgenic line carrying GFP-RHD2 plasmolyzed by 300 mM mannitol **(M)** that was before stained with Amplex Red **(N)**, shown in merged image **(O)**. Scale bar = 10 µm **(A-O)**.

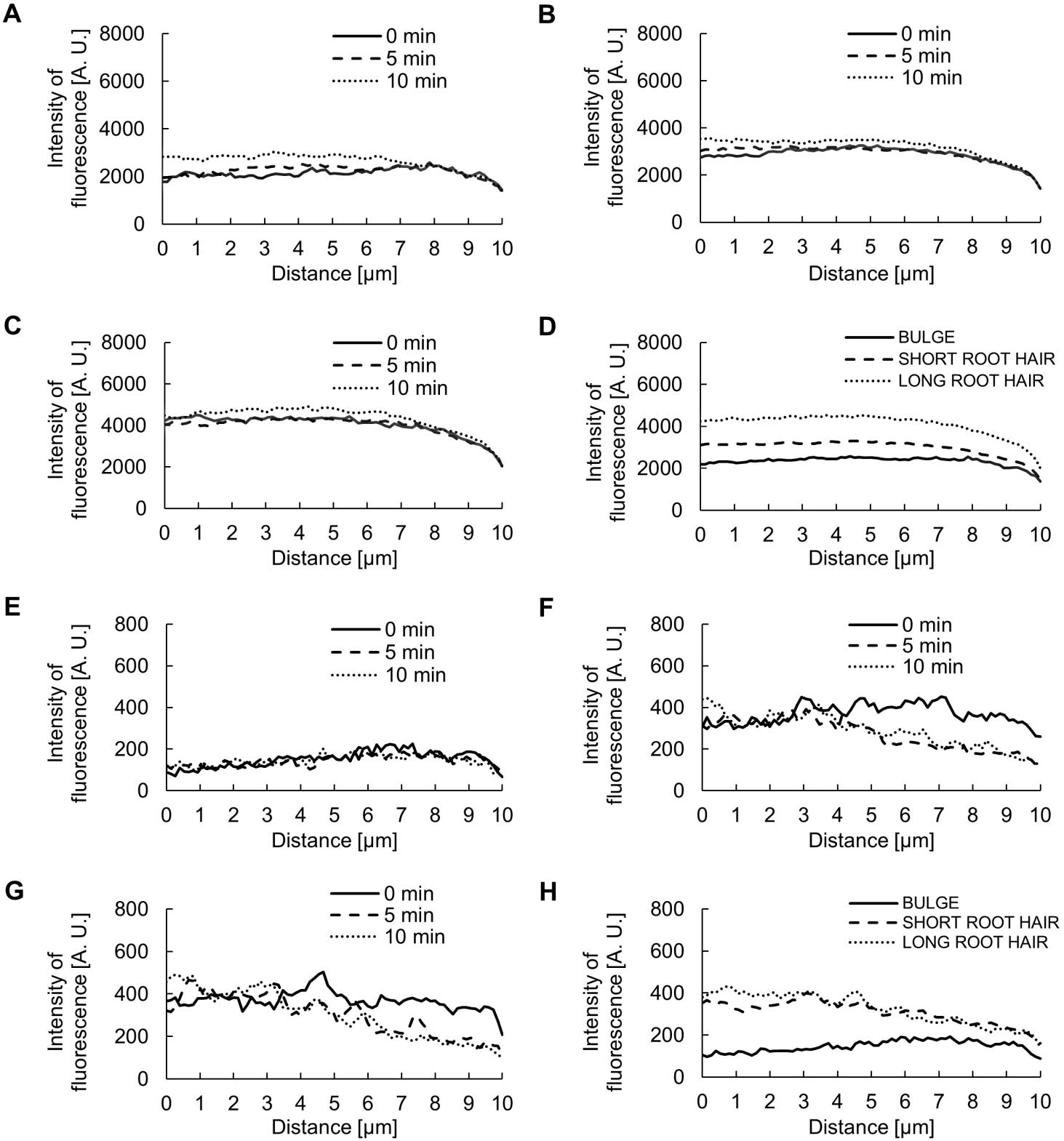

Figure 4. Fluorescence intensity profiles in apical parts of bulges and root hairs after ROS staining with CM-H_2DCFDA and CellRox Deep Red. A-D. Mean fluorescence intensity distribution of CM-H_2DCFDA measured along a 10 µm line oriented longitudinally at the central part, reaching the apical cell wall (schematically illustrated in Materials and Methods) in bulges **(A)**, „short“ **(B)** and „long“ **(C)** growing root hairs. Mean fluorescence intensities were measured at 0 min, 5 min and 10 min of imaging **(A-C)**. **D.** Differences in mean fluorescence intensities of CM-H_2DCFDA measured during root hair development from bulges to „long“ root hairs. **E-H.** Mean fluorescence intensity distribution of CellRox Deep Red measured along a 10 µm line oriented longitudinally at the central part, reaching the apical cell wall in bulges **(E)** „short“ **(F)** and „long“ **(G)** growing root hairs. Mean fluorescence intensities were measured at 0 min, 5 min and 10 min of imaging **(E-G)**. **H.** Differences in mean fluorescence intensities of CellRox Deep Red measured during root hair development from bulges to „long“ root hairs.

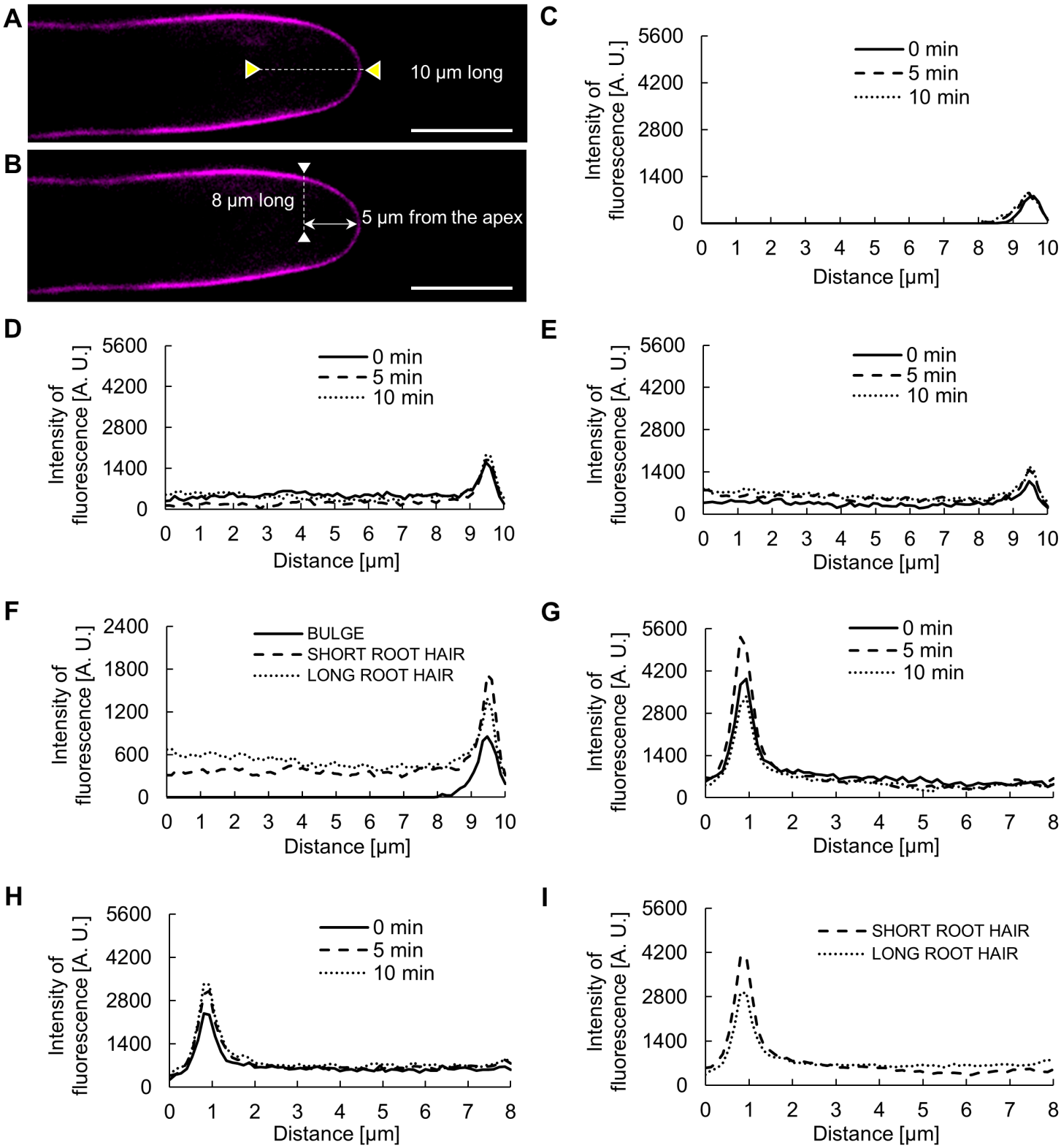

Figure 5. Fluorescence intensity profiles in apical parts of bulges and root hairs after ROS staining with Amplex Red. A-B. Location of a profile 10 µm long for fluorescence intensity measurement in the longitudinal direction **(A)** and a profile 8 µm long in a distance of 5 µm from the apical cell wall for fluorescence intensity measurement in the transversal direction **(B)**. **C-F.** Mean fluorescence intensity distribution of Amplex Red measured along a 10 µm line oriented longitudinally at the central part, reaching the apical cell wall (according to **A**) in bulges **(C)**, „short“ **(D)** and „long“ **(E)** growing root hairs. **F.** Differences in mean fluorescence intensities of Amplex Red measured in longitudinal direction during root hair development from bulges to „long“ root hairs. **G-I.** Mean fluorescence intensity distribution of Amplex Red measured transversally (according to **B**) in „short“ **(G)** and „long“ **(H)** growing root hairs. **I.** Differences in mean fluorescence intensities of Amplex Red measured in transversal direction between „short“ and „long“ root hairs. Mean fluorescence intensities were measured at 0 min, 5 min and 10 min of imaging. Scale bar = 10 µm **(A,B)**.

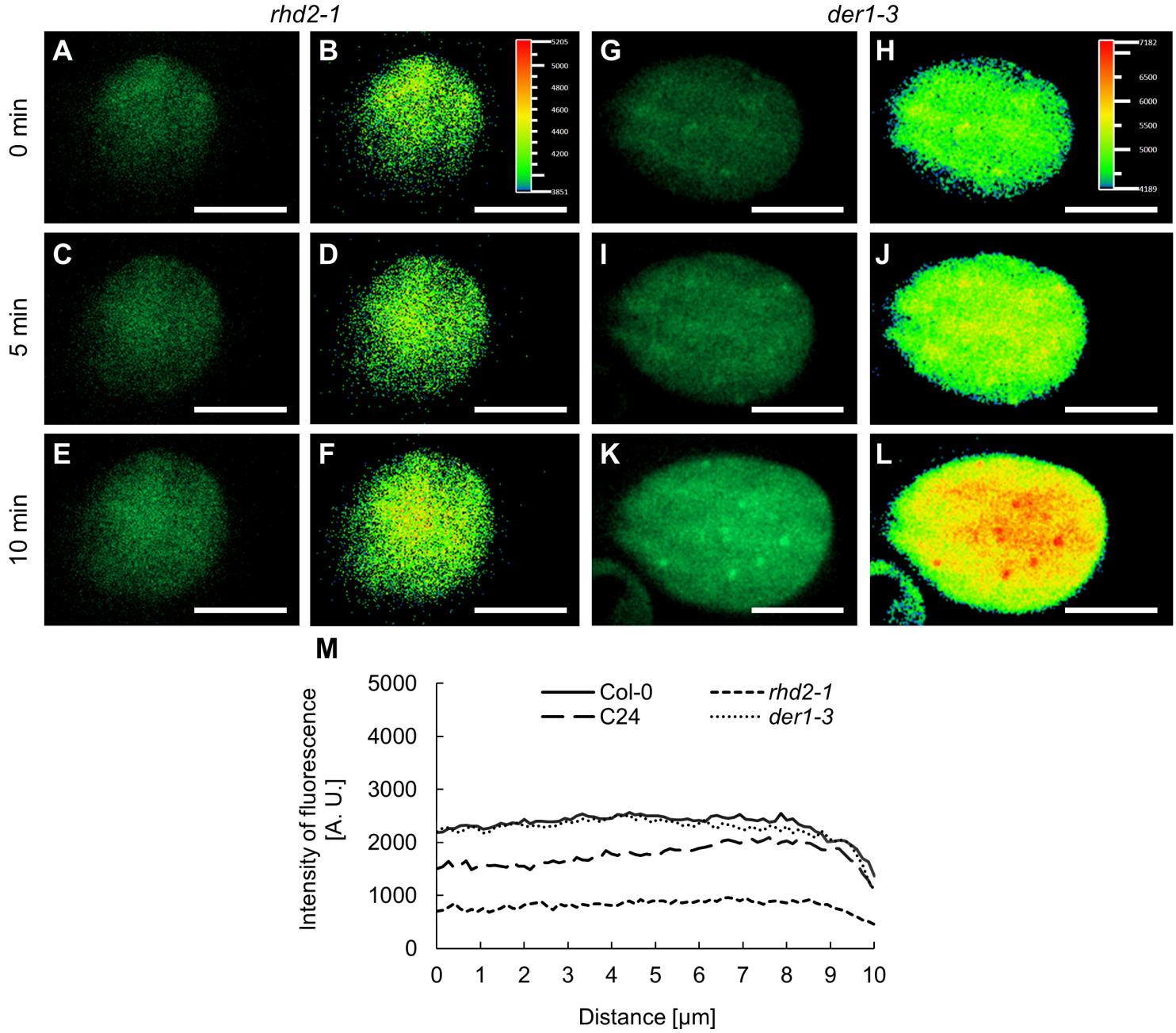

Figure 6. Distribution of ROS after staining with CM-H_2DCFDA in bulges of *rhd2-1* and *der1-3* mutants. A-F. Bulge in *rhd2-1* mutant illustrated at time points of 0 min **(A,B)**, 5 min **(C,D)** and 10 min **(E,F)** of imaging. **G-L.** Bulge in *der1-3* mutant illustrated at time points of 0 min **(G,H)**, 5 min **(I,J)** and 10 min **(K,L)** of imaging. Semi-quantitative fluorescence intensity distribution in *rhd2-1* mutant **(B,D,F)** and *der1-3* mutant **(H,J,L)** is visualized in a pseudo-color-coded scale, where dark blue represents minimal intensity and pale red represents maximum intensity (insets in **B** and **H**). Image acquisition at the time point 0 min started 101 min and 49 min after probe application in *rhd2-1* mutant and *der1-3* mutant, respectively. **M.** Differences in mean fluorescence intensities of CM-H_2DCFDA in *rhd2-1* and *der1-3* mutants, and respective Col-0 and C24 wild-types, measured along a 10 µm line oriented longitudinally at the central part of bulges. Scale bar = 10 µm **(A-L)**.

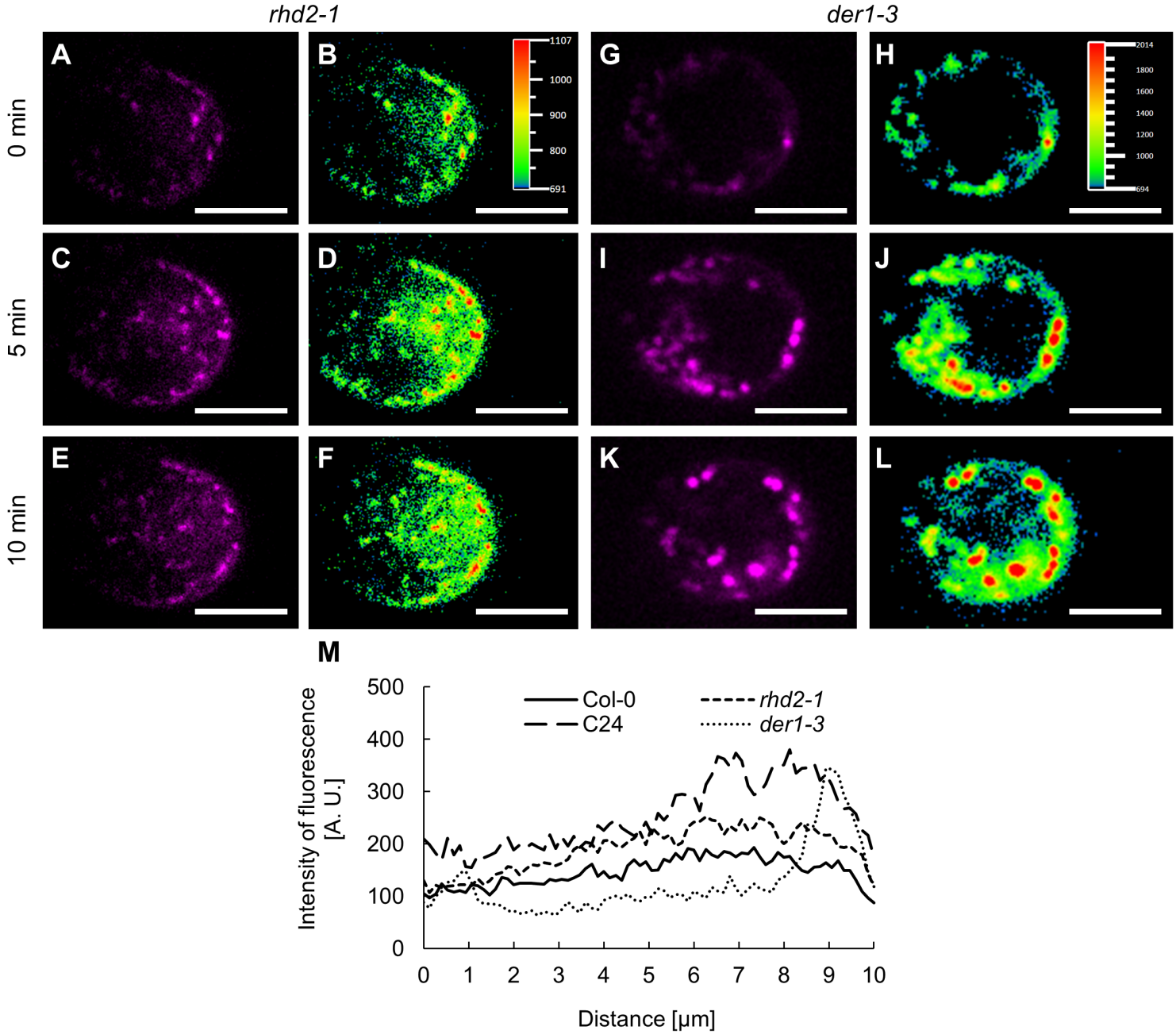

Figure 7. Distribution of ROS after staining with CellRox Deep Red in bulges of *rhd2-1* and *der1-3* mutants. A-F. Bulge in *rhd2-1* mutant illustrated at time points of 0 min **(A,B)**, 5 min **(C,D)** and 10 min **(E,F)** of imaging. **G-L.** Bulge in *der1-3* mutant illustrated at time points of 0 min **(G,H)**, 5 min **(I,J)** and 10 min **(K,L)** of imaging. Semi-quantitative fluorescence intensity distribution in *rhd2-1* mutant **(B,D,F)** and *der1-3* mutant **(H,J,L)** is visualized in a pseudo-color-coded scale, where dark blue represents minimal intensity and pale red represents maximum intensity (insets in **B** and **H**). Image acquisition at the time point 0 min started 74 min and 7 min after probe application in *rhd2-1* mutant and *der1-3* mutant, respectively. **M.** Differences in mean fluorescence intensities of CellRox Deep Red in *rhd2-1* and *der1-3* mutants, and respective Col-0 and C24 wild-types, measured along a 10 µm line oriented longitudinally at the central part of bulges. Scale bar = 10 µm **(A-L)**.

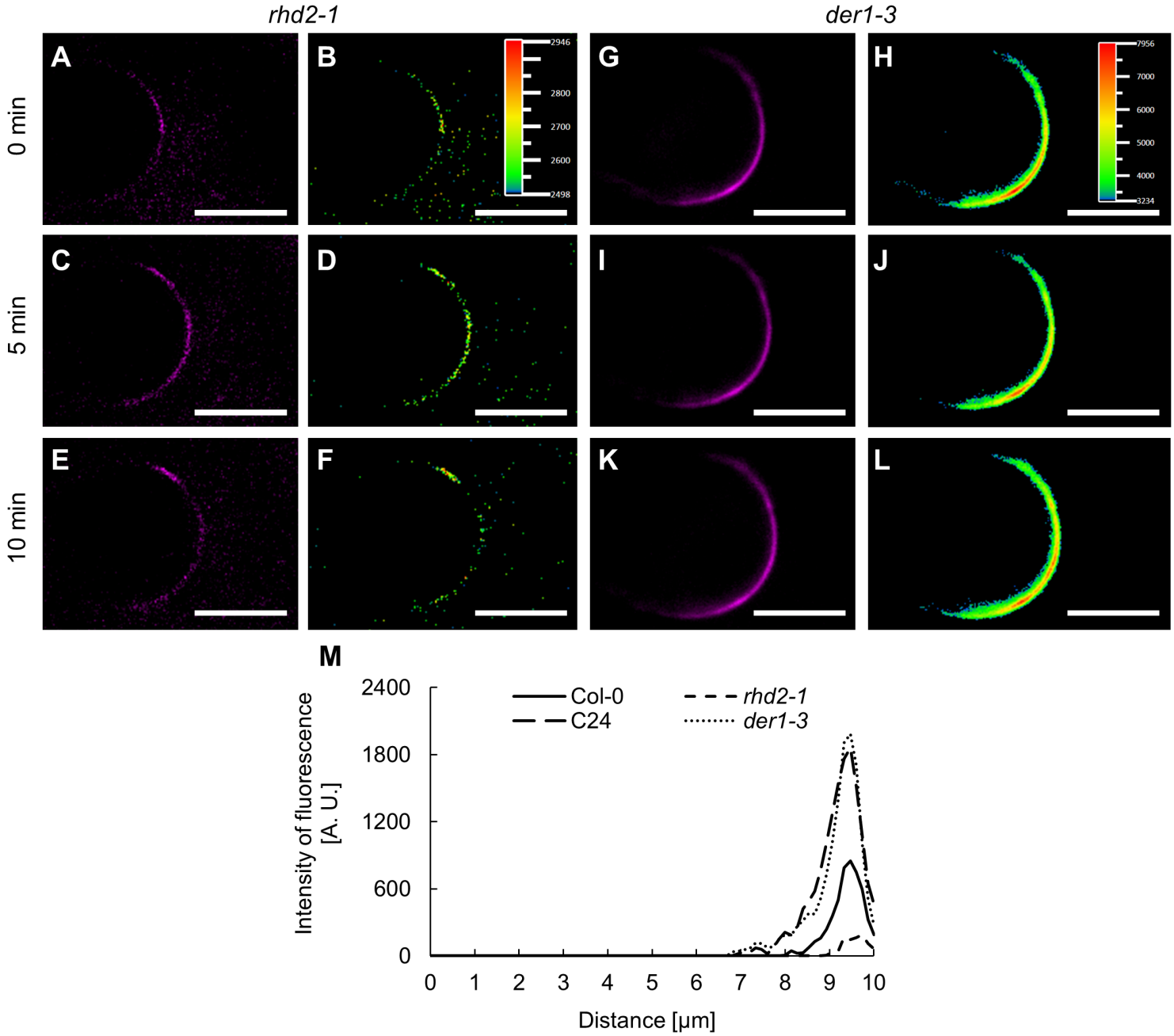

Figure 8. Distribution of ROS after staining with Amplex Red in bulges of *rhd2-1* and *der1-3* mutants. **A-F.** Bulge in *rhd2-1* mutant illustrated at time points of 0 min **(A,B)**, 5 min **(C,D)** and 10 min **(E,F)** of imaging. **G-L.** Bulge in *der1-3* mutant illustrated at time points of 0 min **(G,H)**, 5 min **(I,J)** and 10 min **(K,L)** of imaging. Semi-quantitative fluorescence intensity distribution in *rhd2-1* mutant **(B,D,F)** and *der1-3* mutant **(H,J,L)** is visualized in a pseudo-color-coded scale, where dark blue represents minimal intensity and pale red represents maximum intensity (insets in **B** and **H**). Image acquisition at the time point 0 min started 5 min and 29 min after probe application in *rhd2-1* mutant and *der1-3* mutant, respectively. **M.** Differences in mean fluorescence intensities of Amplex Red in *rhd2-1* and *der1-3* mutants, and respective Col-0 and C24 wild-types, measured along a 10 µm line oriented longitudinally at the central part of bulges. Scale bar = 10 µm **(A-L)**.

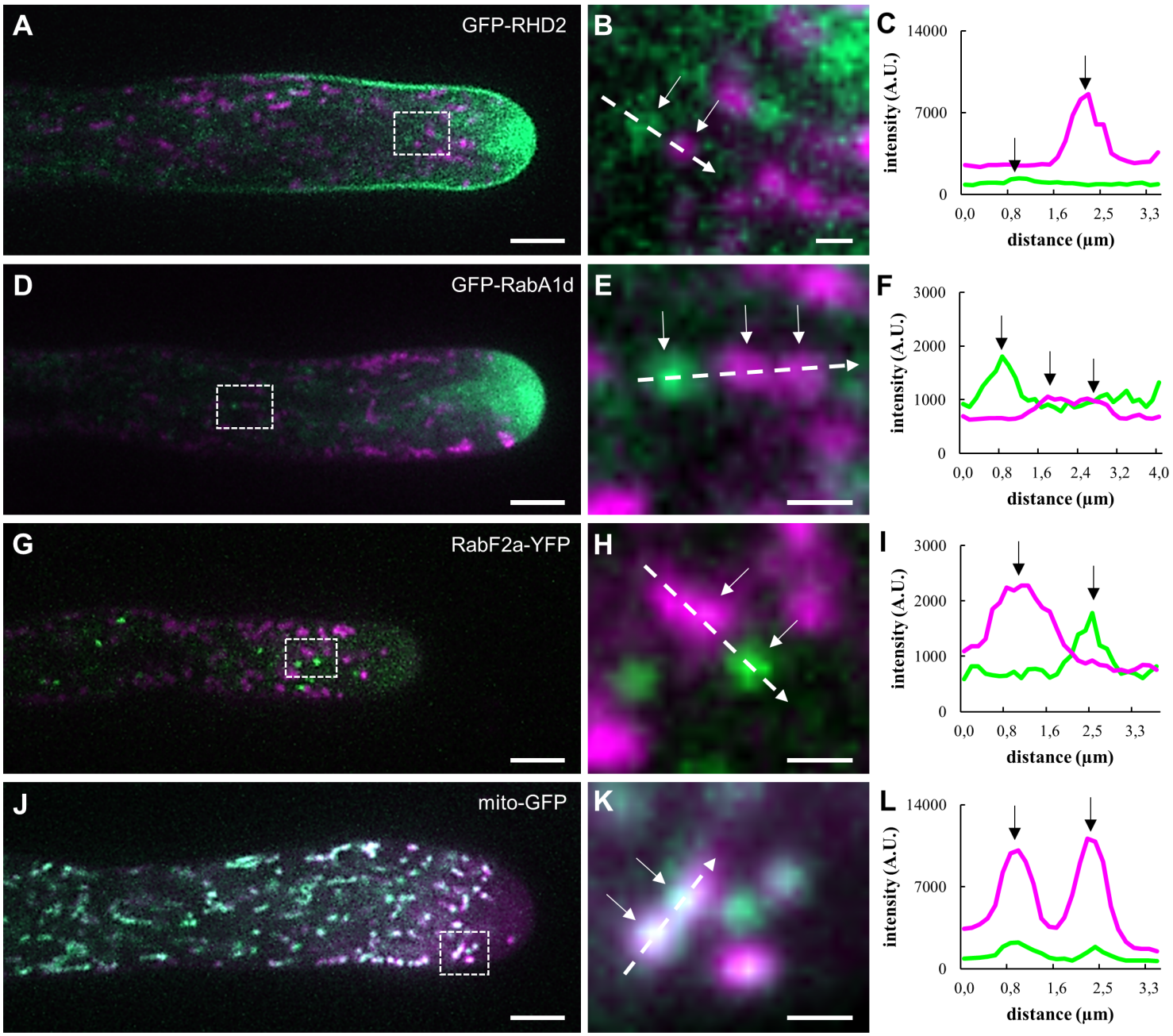

Figure 9. Colocalization analysis of subcellular molecular markers in root hairs with compartments accumulating ROS after staining with CellRox Deep Red. A-C. Colocalization with transgenic line for visualization of vesicular compartments containing GFP-RHD2, a GFP-tagged AtRBOHC/RHD2. **D-F.** Colocalization with transgenic line carrying early endosomal marker GFP-RabA1d. **G-I.** Colocalization with transgenic line carrying late endosomal marker RabF2a-YFP. **J-L.** Colocalization with transgenic line carrying GFP-tagged mitochondria. Overview of root hairs carrying molecular markers (in green) and ROS-accumulating compartments (in magenta) after CellRox Deep Red staining **(A,D,G,J)**. Detailed images of compartments containing carrying molecular markers and ROS **(B,E,H,K)** from the white boxes shown in **(A,D,G,J)**. Fluorescence intensity profiles **(C,F,I,L)** of fluorescence signals of molecular markers (green lines) and ROS-containing compartments (magenta lines) along the interrupted white lines shown in **(B,E,H,K)**. Arrows in **(B,C,E,F,H,I,K,L)** indicate the position of the compartments. Scale bar = 5 µm **(A,D,G,J),** 1 µm **(B,E,H,K)**.

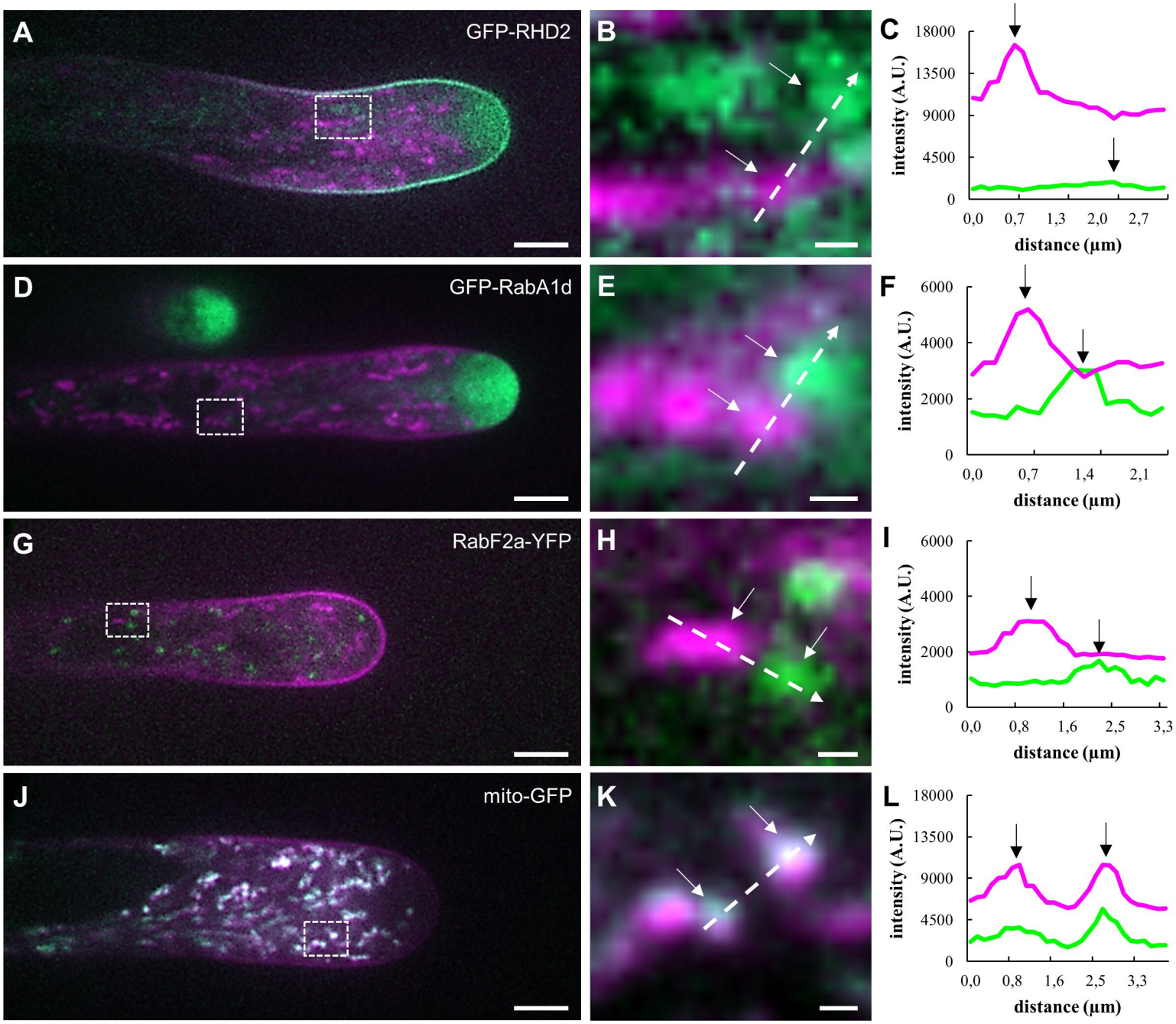

Figure 10. Colocalization analysis of subcellular molecular markers in root hairs with compartments accumulating ROS after staining with Amplex Red. A-C. Colocalization with transgenic line for visualization of vesicular compartments containing GFP-RHD2, a GFP-tagged AtRBOHC/RHD2. **D-F.** Colocalization with transgenic line carrying early endosomal marker GFP-RabA1d. **G-I.** Colocalization with transgenic line carrying late endosomal marker RabF2a-YFP. **J-L.** Colocalization with transgenic line carrying GFP-tagged mitochondria. Overview of root hairs carrying molecular markers (in green) and ROS-accumulating compartments (in magenta) after Amplex Red staining **(A,D,G,J)**. Detailed images of compartments containing carrying molecular markers and ROS **(B,E,H,K)** from the white boxes shown in **(A,D,G,J)**. Fluorescence intensity profiles **(C,F,I,L)** of fluorescence signals of molecular markers (green lines) and ROS-containing compartments (magenta lines) along the interrupted white lines shown in **(B,E,H,K)**. Arrows in **(B,C,E,F,H,I,K,L)** indicate the position of the compartments. Scale bar = 5 µm **(A,D,G,J),** 0.5 µm **(B,E,H,K)**.

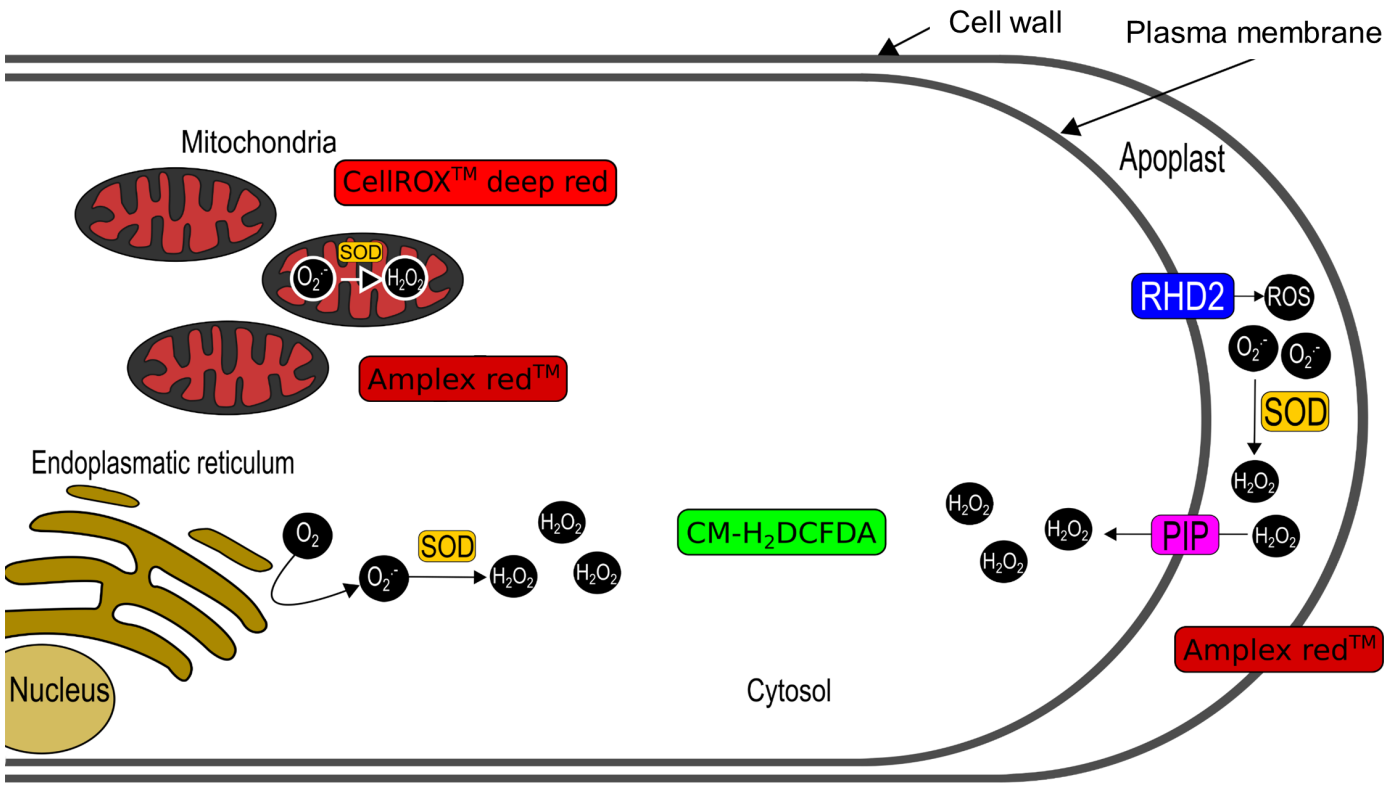

Figure 11. Model of subcellular ROS localization in root hairs with CM-H_2DCFDA, CellRox Deep Red and Amplex Red. CM-H_2DCFDA represents a sensitive probe for ROS (mainly H_2O_2) in the cytoplasm. CellRox Deep Red localizes specifically ROS in mitochondria. Amplex Red serves as a highly sensitive marker for root hair-specific apoplastic ROS (mainly H_2O_2). In addition, root hairs are able to internalize Amplex Red, which sensitively detects H_2O_2 in mitochondria.

Parsed Citations

Alves MBR, de Andrade AFC, de Arruda RP, Batissaco L, Florez- Rodriguez SA, et al. (2015) An Efficient Technique to Detect Sperm Reactive Oxygen Species: The CellRox Deep Red® Fluorescent Probe. Biochem Physiol 4:157
Google Scholar: Author Only Title Only Author and Title

Baluška F, Salaj J, Mathur J, Braun M, Jasper F, Šamaj J, Chua NH, Barlow PW, Volkmann D (2000) Root hair formation: F-actin-independent tip growth is initiated by local assembly of proflin-supported F-actin meshworks accumulated within expansin-enriched bulges. Dev Biol 227: 618-632
Google Scholar: Author Only Title Only Author and Title

Berson T, Wangenheim D, Takáč T, Šamajová O, Rosero A, Ovečka M, Komis G, Stelzer EH, Šamaj J (2014) Trans-Golgi network localized small GTPase RabA1d is involved in cell plate formation and oscillatory root hair growth. BMC Plant Biol 14: 252
Google Scholar: Author Only Title Only Author and Title

Bibikova TN, Zhigilei A, Gilroy S (1997) Root hair growth in Arabidopsis thaliana is directed by calcium and an endogenous polarity. Planta 203: 495–505
Google Scholar: Author Only Title Only Author and Title

Bibikova TN, Jacob T, Dahse I, Gilroy S (1998) Localized changes in apoplastic and cytoplasmic pH are associated with root hair development in Arabidopsis thaliana. Development 125: 2925–2934
Google Scholar: Author Only Title Only Author and Title

Bienert GP, Chaumont F (2014) Aquaporin-facilitated transmembrane diffusion of hydrogen peroxide. Biochim Biophys Acta 1840: 1596–1604
Google Scholar: Author Only Title Only Author and Title

Braun M, Baluška F, von Witsch M, Menzel D (1999) Redistribution of actin, profilin and phosphatidylinositol-4,5-bisphosphate (PIP2) in growing and maturing root hairs. Planta 209: 435–443
Google Scholar: Author Only Title Only Author and Title

Carol RJ, Takeda S, Linstead P, Durrant MC, Kakesova H, Derbyshire P, Drea S, Žárský V, Dolan L (2005) A RhoGDP dissociation inhibitor spatially regulates growth in root hair cells. Nature 438: 1013-1016
Google Scholar: Author Only Title Only Author and Title

Datt JF, Pellinen R, Beeckman T, Van De Cotte B, Langebartels C, Kangasjervi J, Inze D, Van Breusegem F (2003) Changes in hydrogen peroxide homeostasis trigger an active cell death process in tobacco. Plant J 33: 621–629
Google Scholar: Author Only Title Only Author and Title

Demidchik V (2018) ROS-activated ion channels in plants: Biophysical characteristics, physiological functions and molecular nature. Int J Mol Sci 19: E1263
Google Scholar: Author Only Title Only Author and Title

Do THT, Choi H, Palmgren M, Martinoia E, Hwang JU, Lee Y (2019) Arabidopsis ABCG28 is required for the apical accumulation of reactive oxygen species in growing pollen tubes. Proc Nat Acad Sci USA 116: 12540–12549
Google Scholar: Author Only Title Only Author and Title

Dolan L, Duckett C, Grierson C, Linstead P, Schneider K, Lawson E, Dean C, Poethig S, Roberts K (1994) Clonal relationships and cell patterning in the root epidermis of Arabidopsis. Development 120: 2465-2474
Google Scholar: Author Only Title Only Author and Title

Eruslanov E, Kusmartsev S (2010) Identification of ROS using oxidized DCFDA and flow-cytometry. Methods in Molecular Biology 594: 57-72
Google Scholar: Author Only Title Only Author and Title

Foreman J, Demidchik V, Bothwell JH, Mylona P, Miedema H, Torres MA, Linstead P, Costa S, Brownlee C, Jones JD, Davies JM, Dolan L (2003) Reactive oxygen species produced by NADPH oxidase regulate plant cell growth. Nature 422: 442–446
Google Scholar: Author Only Title Only Author and Title

Gilroy S, Jones DL (2000) Through form to function: root hair development and nutrient uptake. Trends Plant Sci 5: 56–60
Google Scholar: Author Only Title Only Author and Title

Gorgidze LA, Oshemkova SA, Vorobjev IA (1998) Blue light inhibits mitosis in tissue culture cells. Bioscience Reports 18: 215-224
Google Scholar: Author Only Title Only Author and Title

Hockberger PE, Skimina TA, Centonze VE, Lavin C, Chu S, Dadras S, Reddy JK, White JG (1999) Activation of flavin-containing oxidases underlies light-induced production of H2O2 in mammalian cells. Proc Nat Acad Sci USA 96: 6255-6260.
Google Scholar: Author Only Title Only Author and Title

Hoffman A, Spetner LM, Burke M (2008) Ramifications of a Redox Switch within a Normal Cell; Its Absence in a Cancer Cell. Free

Radical Biology and Medicine 45: 265–268
Google Scholar: Author Only Title Only Author and Title

Cho H-T, Cosgrove DJ (2002) Regulation of root hair initiation and expansin gene expression in Arabidopsis. Plant Cell 14: 3237–3253
Google Scholar: Author Only Title Only Author and Title

Icha J, Weber M, Waters JC, Norden C (2017) Phototoxicity in live fluorescence microscopy, and how to avoid it. BioEssays 39(8)
Google Scholar: Author Only Title Only Author and Title

Kalyanaraman B, Darley-Usmar V, Davies KJ, Dennery PA, Forman HJ, Grisham MB, Mann GE, Moore K, Roberts LJ 2nd, Ischiropoulos H (2012) Measuring reactive oxygen and nitrogen species with fluorescent probes: challenges and limitations. Free Radical Biology & Medicine 52: 1-6
Google Scholar: Author Only Title Only Author and Title

Khan I, Tang E, Arany P (2015) Molecular pathway of near-infrared laser phototoxicity involves ATF-4 orchestrated ER stress. Scientific Reports 5:10581
Google Scholar: Author Only Title Only Author and Title

Kuběnová L, Tichá M, Šamaj J, Ovečka M (2022) ROOT HAIR DEFECTIVE 2 vesicular delivery to the apical plasma membrane domain during Arabidopsis root hair development. Plant Physiol 188: 1563-1585
Google Scholar: Author Only Title Only Author and Title

Lee Y, Bak G, Choi Y, Chuang WI, Cho HT, Lee Y (2008) Roles of Phosphatidylinositol 3-Kinase in Root Hair Growth. Plant Physiol 147: 624–635
Google Scholar: Author Only Title Only Author and Title

Leshem Y, Seri L, Levine A (2007) Induction of phosphatidylinositol 3-kinase-mediated endocytosis by salt stress leads to intracellular production of reactive oxygen species and salt tolerance. Plant J 51: 185–197
Google Scholar: Author Only Title Only Author and Title

Mangano S, Juárez SPD, Estevez JM (2016) ROS Regulation of Polar Growth in Plant Cells. Plant Physiol 171: 1593-1605
Google Scholar: Author Only Title Only Author and Title

Miedema H, Demidchik V, Véry AA, Bothwell JH, Brownlee C, Davies JM (2008). Two voltage-dependent calcium channels co-exist in the apical plasma membrane of Arabidopsis thaliana root hairs. New Phytologist 179: 378-385
Google Scholar: Author Only Title Only Author and Title

Mittler R (2017) ROS are good. Trends Plant Sci 22: 11–19
Google Scholar: Author Only Title Only Author and Title

Mittler R, Zandalinas SI, Fichman Y, Van Breusegem F (2022) Reactive oxygen species signalling in plant stress responses. Nature Rev Mol Cell Biol 23: 663-679
Google Scholar: Author Only Title Only Author and Title

Murphy MP, Bayir H, Belousov V, Chang CJ, Davies KJA, Davies MJ, Dick TP, Finke T, Forman HJ, Janssen-Heininger Y, et al., (2022) Guidelines for measuring reactive oxygen species and oxidative damage in cells and in vivo. Nat Metabolism 4: 651–662
Google Scholar: Author Only Title Only Author and Title

Niwa Y, Hirano T, Yoshimoto K, Shimizu M, Kobayashi H (1999) Non-invasive quantitative detection and applications of nontoxic, S65T-type green fluorescent protein in living cells. Plant J 18: 455–463
Google Scholar: Author Only Title Only Author and Title

Ovečka M, Berson T, Beck M, Derksen J, Šamaj J, Baluška F, Lichtscheidl IK (2010) Structural sterols are involved in both the initiation and tip growth of root hairs in Arabidopsis thaliana. Plant Cell 22: 2999–3019
Google Scholar: Author Only Title Only Author and Title

Ovečka M, Lichtscheidl I, Šamaj J (2014) Live microscopy analysis of endosomes and vesicles in tip-growing root hairs. Methods Mol Biol 1209: 31–44
Google Scholar: Author Only Title Only Author and Title

Pei W, Du F, Zhang Y, He T, Ren H (2012) Control of the actin cytoskeleton in root hair development. Plant Sci 187: 10–18
Google Scholar: Author Only Title Only Author and Title

Potocký M, Jones MA, Bezvoda R, Smirnoff N, Žárský V (2007) Reactive oxygen species produced by NADPH oxidase are involved in pollen tube growth. New Phytol 174: 742–751
Google Scholar: Author Only Title Only Author and Title

Reszka KJ, Wagner BA, Burns CP, Britigan BE (2005) Effects of peroxidase substrates on the Amplex red/peroxidase assay: antioxidant properties of anthracyclines. Anal Biochem 342: 327-337
Google Scholar: Author Only Title Only Author and Title

Ringli C, Baumberger N, Diet A, Frey B, Keller B (2002) ACTIN2 is essential for bulge site selection and tip growth during root hair development of Arabidopsis. Plant Physiol 129: 1464-1472
Google Scholar: Author Only Title Only Author and Title

Rösner J, Liotta A, Angamo EA, Spies C, Heinemann U, Kovács R (2016) Minimizing photodecomposition of flavin adenine dinucleotide fluorescence by the use of pulsed LEDs. Journal of Microscopy 264: 215-223
Google Scholar: Author Only Title Only Author and Title

Schiefelbein JW, Somerville C (1990) Genetic control of root hair development in Arabidopsis thaliana. Plant Cell 2: 235–243
Google Scholar: Author Only Title Only Author and Title

Smirnoff N, Arnaud D (2019) Hydrogen peroxide metabolism and functions in plants. New Phytol 221: 1197–1214
Google Scholar: Author Only Title Only Author and Title

Staiger CJ, Gibbon BC, Kovar DR, Zonia LE (1997) Profilin and actin depolymerizing factor: modulators of actin organization in plants. Trends Plant Sci 2: 275–281
Google Scholar: Author Only Title Only Author and Title

Swanson SJ, Choi WG, Chanoca A, Gilroy S (2011) In vivo imaging of Ca2+, pH, and reactive oxygen species using fluorescent probes in plants. Annu Rev Plant Biol 62: 273–297
Google Scholar: Author Only Title Only Author and Title

Šamaj J, Müller J, Beck M, Böhm N, Menzel D (2006) Vesicular trafficking, cytoskeleton and signalling in root hairs and pollen tubes. Trends Plant Sci 11: 594-600
Google Scholar: Author Only Title Only Author and Title

Takeda S, Gapper C, Kaya H, Bell E, Kuchitsu K, Dolan L (2008). Local positive feedback regulation determines cell shape in root hair cells. Science 319: 1241–1244
Google Scholar: Author Only Title Only Author and Title

Vaškebová L, Šamaj J, Ovečka M (2018) Single-point ACT2 gene mutation in the Arabidopsis root hair mutant der1-3 affects overall actin organization, root growth and plant development. Ann Bot 122: 889-901
Google Scholar: Author Only Title Only Author and Title

Vissenberg K, Fry SC, Verbelen JP (2001) Root hair initiation is coupled to a highly localized increase of xyloglucan endotransglycosylase action in Arabidopsis roots. Plant Physiol 127: 1125–1135
Google Scholar: Author Only Title Only Author and Title

von Wangenheim D, Rosero A, Komis G, Šamajová O, Ovečka M, Voigt B, Šamaj J (2016) Endosomal interactions during root hair growth. Front Plant Sci 6: 1262
Google Scholar: Author Only Title Only Author and Title

Wang Y, Zhu Y, Ling Y, Zhang H, Liu P, Baluška F, Šamaj J, Lin J, Wang Q (2010) Disruption of actin filaments induces mitochondrial Ca2+ release to the cytoplasm and [Ca2+]c changes in Arabidopsis root hairs. BMC Plant Biol 10: 53
Google Scholar: Author Only Title Only Author and Title

Winterbourn CC (2014) The challenges of using fluorescent probes to detect and quantify specific reactive oxygen species in living cells. Biochimica et Biophysica Acta 1840: 730-738
Google Scholar: Author Only Title Only Author and Title

Yao N, Tada Y, Sakamoto M, Nakayashiki H, Park P, Tosa Y, Mayama S (2002) Mitochondrial oxidative burst involved in apoptotic response in oats. Plant J 30: 567–579
Google Scholar: Author Only Title Only Author and Title

Zheng M, Beck M, Müller J, Wang X, Wang Q, Baluška F, Logan DC, Šamaj J, Lin J (2009) Cytoskeleton-dependent mitochondrial movements in Arabidopsis root hairs. PLoS One 4:e5961, 1–14
Google Scholar: Author Only Title Only Author and Title